Microstructure-related Stoneley waves and their effect on the scattering properties of a 2D Cauchy/relaxed-micromorphic interface

Alexios Aivaliotis[a,*], Ali Daouadji[a], Gabriele Barbagallo[a], Domenico Tallarico[a], Patrizio Neff[b], Angela Madeo[a]

[a] *GEOMAS, INSA-Lyon, Université de Lyon, 20 avenue Albert Einstein, 69621, Villeurbanne cedex, France*
[b] *Head of Chair for Nonlinear Analysis and Modelling, Fakultät für Mathematik, Universität Duisburg-Essen, Mathematik-Carrée, Thea-Leymann-Straße 9, 45127 Essen, Germany*

Abstract

In this paper we set up the full two-dimensional plane wave solution for scattering from an interface separating a classical Cauchy medium from a relaxed micromorphic medium. Both media are assumed to be isotropic and semi-infinite to ease the semi-analytical implementation of the associated boundary value problem.

Generalized macroscopic boundary conditions are presented (continuity of macroscopic displacement, continuity of generalized tractions and, eventually, additional conditions involving purely microstructural constraints), which allow for the effective description of the scattering properties of an interface between a homogeneous solid and a mechanical metamaterial. The associated "generalized energy flux" is introduced so as to quantify the energy which is transmitted at the interface via a simple scalar, macroscopic quantity.

Two cases are considered in which the left homogeneous medium is "stiffer" and "softer" than the right metamaterial and the transmission coefficient is obtained as a function of the frequency and of the direction of propagation of the incident wave. We show that the contrast of the macroscopic stiffnesses of the two media, together with the type of boundary conditions, strongly influence the onset of Stoneley (or evanescent) waves at the interface. This allows for the tailoring of the scattering properties of the interface at both low and high frequencies, ranging from zones of complete transmission to zones of zero transmission well beyond the band-gap region.

Keywords: enriched continua, metamaterials, band-gaps, wave-propagation, Stoneley waves, relaxed micromorphic model, interface, total reflection and transmission

AMS 2010 subject classification: 74A30 (nonsimple materials), 74A60 (micromechanical theories), 74B05 (classical linear elasticity), 74J05 (linear waves), 74J10 (bulk waves), 75J15 (surface waves), 74J20 (wave scattering), 74M25 (micromechanics).

*Corresponding author

Email addresses: alexios.aivaliotis@insa-lyon.fr (Alexios Aivaliotis), ali.daouadji@insa-lyon.fr (Ali Daouadji), gabriele.barbagallo@insa-lyon.fr (Gabriele Barbagallo), domenico.tallarico@insa-lyon.fr (Domenico Tallarico), patrizio.neff@uni-due.de (Patrizio Neff), angela.madeo@insa-lyon.fr (Angela Madeo)

1. Introduction

Recent years have seen the rapid development of acoustic metamaterials whose mechanical properties allow exotic material behaviors such as band-gaps (20; 41; 44), cloaking (8; 6; 29; 40), focusing (11; 15; 38), wave-guiding (16; 39) etc. If the bulk behavior of these metamaterials has gathered the attention of the scientific community via the application of discrete modeling (such as Bloch-Floquet analysis or homogenization techniques (10; 35; 42; 19)) or, more recently, of enriched continuum models (4; 12; 21; 22; 23; 24; 25; 26; 27; 28; 30; 31; 32), the study of the reflective/refractive properties at the boundary of such metamaterials is far from being well understood. Rare examples of the study of scattering phenomena at metamaterials boundaries in the framework of classical homogenization approaches can be found in (5; 7; 36; 42; 43).

On the other hand, good knowledge of the reflective and transmittive properties of such interfaces could be a key point for the conception of metamaterial systems, which would completely transform the idea we currently have about reflection and transmission of elastic waves at the interface between two solids. It is for this reason that many authors convey their research towards what they call "metasurfaces" (18; 17; 45), i.e. relatively thin layers of metamaterials whose microstructure is able to interact with the incident wave-front in such a way that the resulting reflection/transmission patterns exhibit exotic properties, such as total reflection or total transmission, conversion of a bulk incident wave in interface waves, etc.

Notwithstanding the paramount importance these metasurfaces may have for technological advancements in the field of noise absorption or stealth, they show limitations in the sense that they work for relatively small frequency ranges, for which the wavelength of the incident wave is comparable to the thickness of the metasurface itself. This restricts the range of applicability of such devices, above all for what concerns low frequencies which would result in very thick metasurfaces.

In this paper, we choose a different approach for modeling the reflective and diffractive properties of an interface which separates a bulk homogeneous material from a bulk metamaterial. This interface does not itself contain any internal structure, but its refractive properties can be modulated by suitably tailoring the bulk properties of the two adjacent media and, in particular, their relative macroscopic stiffness. The homogeneous material is modeled via a classical linear-elastic Cauchy model, while the metamaterial is described by the linear relaxed micromorphic model, an enriched continuum model which already proved its effectiveness in the description of the bulk behavior of certain metamaterials (21; 22; 23).

We explicitly point out that the relaxed micromorphic model is not obtained via a direct upscaling approach based, for example, on classical or numerical dynamical homogenization (9; 35; 42). The theoretical framework is set up directly at the macroscopic scale and the homogenized behavior can be mapped back onto specific metamaterials' microstructures via an inverse fitting procedure of the dispersion curves, e.g. on Bloch-Floquet diagrams. If it cannot be expected that the relaxed micromorphic model reproduces point by point the dispersive behavior of real metamaterials, it can, to a very good extent, qualitatively and quantitatively reproduce the averaged properties of such materials, including the metamaterial's dispersion, band-gap and macroscopic scattering.

Concerning the study of metamaterial's boundaries, the relaxed micromorphic model is a powerful tool, which provides coherent macroscopic boundary conditions allowing the study of realistic interface problems.

Previous studies of the authors have provided the foundation of the theoretical basis for the definition of isotropic and anisotropic relaxed micromorphic media, including well-posedness results (13; 31; 30; 33). They have also explored the bulk behavior of such media, starting a comparison

with real metamaterials (23; 22; 27) and have attempted some academic studies of 1D refractive problems at relaxed micromorphic interfaces (22; 28). In the present paper, for the first time, we propose a complete 2D framework for the study of the refractive properties of relaxed micromorphic interfaces. Potentially, this provides powerful tools for advancing towards the validation of the model on real metastructures, in which it is certain that the scattering properties do not only depend on the frequency, but also on the angle of incidence. In this paper, we do not target any specific microstructure, since the proposed results are general and are uniquely driven by the contrast of macroscopic stiffness of the two media on the two sides of the interface. Nevertheless, we point out that the true efficacy of the model lies in the ability of providing boundary conditions (continuity of macroscopic displacement and of "generalized" tractions), which are pertinent at the macroscopic scale.

We are able to clearly show that when the homogeneous material is "stiffer" than the considered metamaterial, zones of very high (sometimes total) transmission can be found at both low and high frequencies. More precisely, we find that high-frequency total transmission is discriminated by a critical angle, beyond which total transmission gradually shifts towards total reflection. Engineering systems of this type could be fruitfully exploited for the conception of wave filters, for non-destructive evaluation or for selective cloaking.

On the other hand, we show that when the homogeneous material is "softer" than the metamaterial, broadband total reflection can be achieved for almost all frequencies and angles of incidence. This could be of paramount importance for the conception of wave screens that are able to isolate regions from noise and/or vibration. We are also able to show that such total reflection phenomena are related to the onset of classical Stoneley interface waves[1] at low frequencies (37) and of new microstructure-related interface waves at higher frequencies.

We underline again the fact that no precise microstructure is targeted in this paper, since the presented results could be re-adjusted for any specific metamaterial without changing the overall results. This is due to the fact that the properties we unveil here only depend on the "relative stiffnesses" of the considered media and not on the absolute stiffness of the metamaterial itself.

1.1. Notation

Let $\mathbb{R}^{3\times3}$ be the set of all real 3×3 second order tensors (matrices) which we denote by capital letters. A simple and a double contraction between tensors of any suitable order is denoted by $\cdot$ and $:$ respectively, while the scalar product of such tensors by $\langle\cdot,\cdot\rangle$. The Einstein sum convention is implied throughout this text unless otherwise specified. The standard Euclidean scalar product on $\mathbb{R}^{3\times3}$ is given by $\langle X,Y\rangle = \mathrm{tr}(X\cdot Y^T)$ and consequently the Frobenius tensor norm is $\|X\|^2 = \langle X,X\rangle$. The identity tensor on $\mathbb{R}^{3\times3}$ will be denoted by $\mathbb{1}$; then, $\mathrm{tr}(X) = \langle X,\mathbb{1}\rangle$.

We denote by B_L a bounded domain in $\mathbb{R}^3$, by ∂B_L its regular boundary and by Σ any material surface embedded in B_L. The outward unit normal to ∂B_L will be denoted by ν as will the outward unit normal to a surface Σ embedded in B_L. Given a field a defined on the surface Σ, we define the jump of a through the surface Σ as:

$$[[a]] = a^+ - a^-, \qquad [a]^- := \lim_{\substack{x\in B_L^-\setminus\Sigma \\ x\to\Sigma}} [a], \qquad \text{with} \qquad [a]^+ := \lim_{\substack{x\in B_L^+\setminus\Sigma \\ x\to\Sigma}} [a], \tag{1.1}$$

[1] Interface waves propagating at the interface between an elastic solid and air are called Rayleigh waves, after Lord Rayleigh, who was the first to show their existence (34). Interface waves propagating at the surface between two solids are called Stoneley waves after R. Stoneley who first showed their existence (37).

with B_L^-, B_L^+ being the two subdomains which result from splitting B_L by the surface Σ.

Classical gradient (∇) and divergence (Div) operators are used throughout the paper. Moreover, we introduce the Curl operator of the matrix P as $(\operatorname{Curl} P)_{ij} = \varepsilon_{jmn} P_{in,m}$, where ε_{jmn} denotes the classical Levi-Civita tensor.

2. Governing equations and energy flux

The equations of motion for a classical, isotropic Cauchy continuum read (see (2)):[2]

$$\rho\, u_{,tt} = \operatorname{Div} \sigma, \qquad \text{with} \qquad \sigma = 2\mu \operatorname{sym} \nabla u + \lambda \operatorname{tr}(\operatorname{sym} \nabla u)\mathbb{1}. \tag{2.1}$$

The equations of motion for an isotropic relaxed micromorphic continuum are (13; 26; 27; 31):[3]

$$\rho\, u_{tt} = \operatorname{Div} \widetilde{\sigma}, \qquad \eta\, P_{tt} = \widetilde{\sigma} - s - \operatorname{Curl} m, \tag{2.2}$$

where

$$\begin{aligned} \widetilde{\sigma} &= 2\mu_e \operatorname{sym}(\nabla u - P) + \lambda_e \operatorname{tr}(\nabla u - P)\, \mathbb{1} + 2\mu_c \operatorname{skew}(\nabla u - P), \\ s &= 2\mu_{\text{micro}} \operatorname{sym} P + \lambda_{\text{micro}} (\operatorname{tr} P)\ \mathbb{1}, \qquad m = \mu_e L_c^2 \operatorname{Curl} P. \end{aligned} \tag{2.3}$$

2.1. Conservation of total energy and energy flux

The mechanical system we are considering is conservative and, therefore, the energy must be conserved in the sense that the following differential form of a continuity equation must hold:

$$E_{,t} + \operatorname{div} H = 0, \tag{2.4}$$

where E is the total energy of the system and H is the energy flux vector. In the case of a classical isotropic Cauchy medium, we have (see (2) for more details):

$$E_{,t} = \operatorname{Div}(\sigma \cdot u_{,t}) \quad \Rightarrow \quad H = -\sigma \cdot u_{,t}. \tag{2.5}$$

On the other hand, when considering a relaxed micromorphic continuum, one has that (see (2)):

$$E_{,t} = \operatorname{Div}\left(\widetilde{\sigma}^T \cdot u_{,t} + \left(m^T \cdot P_{,t}\right) : \varepsilon\right) \quad \Rightarrow \quad H = -\widetilde{\sigma}^T \cdot u_{,t} - \left(m^T \cdot P_{,t}\right) : \varepsilon. \tag{2.6}$$

[2] Following classical notation, $u(x,t)$ denotes the macroscopic displacement field, ρ is the macroscopic density and λ and μ are the Lamé parameters of the Cauchy medium. The tensor $\sigma(x,t)$ is the classical Cauchy stress tensor.

[3] In equations (2.2) the basic kinematical fields are the macroscopic displacement $u(x,t)$ and the micro-distortion tensor $P(x,t)$, which accounts for microstructure-related motions. Moreover, ρ is the macroscopic apparent density of the considered continuum (it accounts for the average volume distribution of the masses of the base constituents when a specific microstructure is targeted), λ_{micro} and μ_{micro} are elastic moduli which can be related to the elastic properties of the unit cell, μ_c is the Cosserat couple modulus and λ_e and μ_e are coefficients which allow the transition from the micro to the macro scale (see (12) for details). Finally, L_c is an internal length, which can account for non-local effects, known to be particularly relevant to microstructures showing a strong contrast between the base materials. Enriching kinematics through the introduction of extra degrees of freedom is at the core of the relaxed micromorphic model's ability to predict the behavior of complex metamaterials. These extra degrees of freedom allow for the description of microstructure-related motions at the level of the unit cell and, when considering a dynamical setting, this translates to being able to account for the presence of optic curves in the dispersion diagrams (see Fig. 3). The isotropic model presented here is used to present general results about the scattering properties of a relaxed micromorphic interface and does not target any specific metamaterial microstructure. To actually fit the relaxed micromorphic model to a real microstructure, we need to generalize it to the general anisotropic case.

3. Boundary conditions

3.1. Boundary conditions on an interface between two classical Cauchy media

As it is well known (see e.g. (1; 14; 28)), the boundary conditions which can be imposed at an interface between two Cauchy media are continuity of displacement and of traction:

$$[[u]] = 0 \Rightarrow u^- = u^+, \qquad [[t]] = 0 \Rightarrow t^- = t^+. \tag{3.1}$$

In equations (3.1), u^- is the macroscopic displacement on the "minus" side, u^+ is the macroscopic displacement on the "plus" side and t^- and t^+ are the surface traction vectors on the "minus" and on the "plus" side, respectively. We recall that in a Cauchy medium, $t = \sigma \cdot \nu$, ν being the outward unit normal to the surface and σ being the Cauchy stress tensor given in (2.1).

3.2. Boundary conditions at a Cauchy/relaxed micromorphic interface

In the framework of continuum modeling, it is essential to provide the boundary conditions which are intrinsically compatible with the associated bulk equations and which provide the well-posedness of the resulting boundary value problem. The correct choice of boundary conditions to be imposed for a specific problem naturally follows when using a variational principle and, for the case of the relaxed micromorphic model, has been deeply studied in previous theoretical works (4; 12; 21; 22; 23; 24; 25; 26; 27; 28; 30; 31; 32).

The first jump conditions, which have to be imposed at a Cauchy/relaxed micromorphic interface are continuity of displacement and of generalized force at the considered interface:

$$u^- = u^+ \qquad \text{and} \qquad t = \widetilde{t}, \tag{3.2}$$

where the "plus" side is occupied by the relaxed micromorphic medium, $t = \sigma \cdot \nu$ is the surface traction calculated on the Cauchy side and the traction for the relaxed micromorphic model is given by $\widetilde{t} = \widetilde{\sigma} \cdot \nu$, $\widetilde{\sigma}$ being given in (2.3). In a relaxed micromorphic continuum, the notion of force has to be generalized. This is achieved through the introduction of the "enriched" stress tensor $\widetilde{\sigma}$ which accounts for both macro and microstructure related deformations.

Equations (3.2) must be complemented with an extra jump condition, which discriminates between what we call "free" and "fixed" microstructure. Both these jump conditions are coherent with the variational principle which is behind the considered relaxed micromorphic model (see (13; 21; 28; 27; 23; 31)). In order to define the two types of boundary conditions we are interested in, we need the concept of double force τ which is the dual quantity of the micro-distortion tensor P and is defined as (28)

$$\tau = -m \cdot \varepsilon \cdot \nu, \tag{3.3}$$

where the involved quantities have been defined in (2.3).

3.2.1. Free microstructure

In this case, the macroscopic displacement is continuous while the microstructure of the medium is free to move at the interface (22; 28; 21). Leaving the interface free to move means that P is arbitrary, which, on the other hand, implies the double force τ must vanish. We have then:

$$[[u_i]] = 0, \quad \widetilde{t}_i - t_i = 0, \quad \tau_{ij} = 0, \quad i = 1,2,3, \ j = 2,3. \tag{3.4}$$

The "free microstructure" boundary conditions are easier to impose than the "fixed microstructure" ones. This is indeed clear, since it is more convenient to avoid constraining the microstructure embedded in the unit cell than imposing a vanishing value of the micro-strain at the interface.

3.2.2. Fixed microstructure

This is the case in which we impose that the microstructure on the relaxed micromorphic side does not vibrate at the interface. The boundary conditions in this case are (28)[4]

$$[[u_i]] = 0, \quad \widetilde{t}_i - t_i = 0, \quad P_{ij} = 0, \quad i = 1, 2, 3, \ j = 2, 3. \tag{3.5}$$

We explicitly remark that the free microstructure boundary condition (3.4) is the only one that permits one to obtain an equivalent Cauchy/Cauchy system when considering low frequencies. Indeed, in this case, since the tensor P is left free, it can adjust itself in order to recover a Cauchy medium in the low-frequency limit. On the other hand, the boundary condition (3.5) imposes an artificial value on P along the interface, so that the effect of the microstructure is forced to be present in the system. It follows that a Cauchy/Cauchy system cannot be recovered as a low-frequency limit of a Cauchy/relaxed micromorphic one when the boundary condition (3.5) is imposed.

4. Reflection and transmission at an interface between two Cauchy media

We start this section by pointing out that it is a simple summary of well established classical results. Nevertheless, this summary is essential for the understanding of the present paper, since it allows us to (i) set up the notation which will be naturally extended when dealing with the relaxed micromorphic medium, and (ii) clearly present the conceptual steps which must be followed in order to solve the interface problem. We will follow exactly the same steps when considering a Cauchy/relaxed micromorphic interface, but the explicit presentation of the intermediate analytical expressions in that case is prohibitive due to their formal complexity. Hence, this section can be skipped by the reader who is uniquely interested in the new developments provided by the paper, but it has to be necessarily addressed by the reader who wants to reproduce the calculations for the Cauchy/relaxed micromorphic interface presented in the next section.

We assume in the following, that the interface between the two media from which an incident wave reflects and refracts is the x_2 axis ($x_1 = 0$), see Fig. 1.

Incident waves propagate from $-\infty$ in the $x_1 < 0$ half-plane towards the interface, reflected waves propagate from the interface towards $-\infty$ in the $x_1 < 0$ half-plane and refracted (or, equivalently, transmitted) waves propagate from the interface towards $+\infty$ in the $x_1 > 0$ half-plane. Since we consider 2D wave propagation, the incident wave can hit the interface at an arbitrary angle.

As it is classical, we will consider both in-plane (in the $(x_1x_2)-$ plane) and out-of-plane (along the x_3 direction) motions. Nevertheless, all the considered components of the displacement will only depend on the x_1, x_2 space components (plane wave hypothesis). We hence write

$$u = (u_1(x_1, x_2, t), u_2(x_1, x_2, t), u_3(x_1, x_2, t))^T. \tag{4.1}$$

We now make a small digression on wave propagation in classical Cauchy media. As pointed out in the beginning of this section, these results are of course well known (see e.g. (1; 14)), however, we present them here in detail following our notation, so that we can naturally extend them over to the relaxed micromorphic model.

[4] We remark that only the tangent part of the double force in (3.4) or of the micro-distortion tensor in (3.5) must be assigned (30; 31). This is peculiar of the relaxed micromorphic model and is related to the fact that only Curl P appears in the energy. In a standard Mindlin-Eringen model, where the whole ∇P appears in the energy, the whole double force τ (or alternatively the whole tensor P) must be assigned at the interface. Finally, in an internal variable model (no derivatives of P in the energy), no conditions on P or τ must be assigned at the interface.

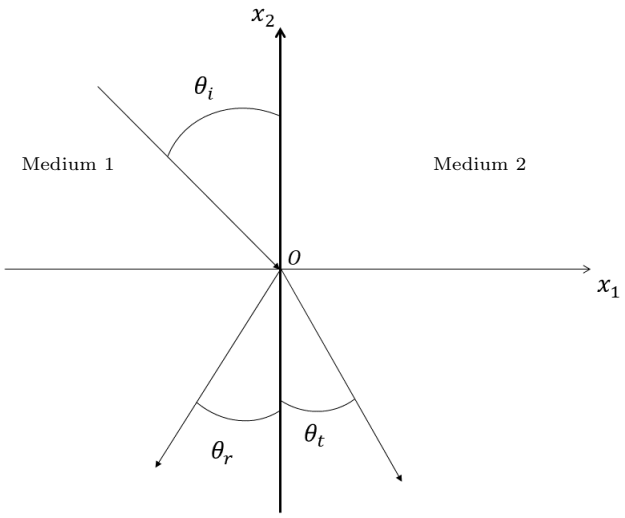

Figure 1: Generic representation of an interface separating two media at $x_1 = 0$. The figure also schematically represents the conventions used for incident, reflected and transmitted waves.

4.1. Wave propagation in bulk Cauchy media

We start by re-writing the governing equations (2.1) by using the plane-wave ansatz. Plugging u as in (4.1) into (2.1) gives:

$$\left.\begin{aligned} \rho\, u_{1,tt} &= (2\mu+\lambda)u_{1,11} + (\mu+\lambda)u_{2,12} + \mu\, u_{1,22} \\ \rho\, u_{2,tt} &= (2\mu+\lambda)u_{2,22} + (\mu+\lambda)u_{1,12} + \mu\, u_{2,11} \end{aligned}\right\} \tag{4.2}$$

$$\rho\, u_{3,tt} = \mu(u_{3,11} + u_{3,22}). \tag{4.3}$$

We remark that the first two equations (4.2) are coupled, while the third (4.3) is not.

We now formulate the plane wave ansatz, according to which:

$$(u_1, u_2)^{\mathrm{T}} = \widehat{\psi}\, e^{i(\langle x,k\rangle - \omega t)} = \widehat{\psi}\, e^{i(x_1k_1 + x_2k_2 - \omega t)}, \quad u_3 = \widehat{\psi}_3\, e^{i(\langle x,k\rangle - \omega t)} = \widehat{\psi}_3\, e^{i(x_1k_1 + x_2k_2 - \omega t)}, \tag{4.4}$$

where $\widehat{\psi} = (\widehat{\psi}_1, \widehat{\psi}_2)^T$ is the vector of amplitudes, $k = (k_1, k_2)^T$ is the wave-vector, which fixes the direction of propagation of the considered wave and $x = (x_1, x_2)^T$ is the position vector. Moreover, $\widehat{\psi}_3$ is a scalar amplitude for the third component of the displacement.

We start by considering the first system of coupled equations and we plug the plane-wave ansatz (4.4) into (4.2), thus obtaining the system of algebraic equations $A \cdot \widehat{\psi} = 0$, where A is the matrix of coefficients

$$A = \begin{pmatrix} \omega^2 - c_L^2 k_1^2 - c_S^2 k_2^2 & -c_V^2 k_1 k_2 \\ -c_V^2 k_1 k_2 & \omega^2 - c_L^2 k_2^2 - c_S^2 k_1^2 \end{pmatrix}, \tag{4.5}$$

and where we defined the abbreviations

$$c_L^2 = \frac{2\mu+\lambda}{\rho}, \qquad c_S^2 = \frac{\mu}{\rho}, \qquad c_V^2 = c_L^2 - c_S^2 = \frac{\mu+\lambda}{\rho}. \tag{4.6}$$

For $A \cdot \widehat{\psi} = 0$ to have a non-trivial solution, we impose $\det A = 0$, which implies (see (2))

$$k_1 = \pm\sqrt{\frac{\omega^2}{c_L^2} - k_2^2} \quad \text{or} \quad k_1 = \pm\sqrt{\frac{\omega^2}{c_S^2} - k_2^2}, \tag{4.7}$$

The first or second solution in (4.7) is associated to what we call a longitudinal (L) or in-plane (SV) shear wave, respectively. The choice of sign for these solutions is related to the direction of propagation of the considered wave (positive for incident and transmitted waves, negative for reflected waves).

We will recall later on that, once boundary conditions are imposed at a given interface between two Cauchy media, the value of the component k_2 of the wave-vector k can be considered to be known. We will see that k_2 is always real and positive, which means that, according to (4.7), the first component k_1 of the wave-vector can be either real or purely imaginary, depending on the values of the frequency and of the material parameters. Two scenarios are then possible:

1. both k_1 and k_2 are real: According to the wave ansatz (4.4), we have a harmonic wave which propagates in the direction given by the wave-vector k lying in the $(x_1x_2)-$ plane.

2. k_2 is real and k_1 purely imaginary: According to equation (4.4), the wave continues to propagate in the x_2 direction (along the interface), but decays with a negative exponential in the x_1 direction (away from the interface). Such a wave is known as a Stoneley wave (37; 3).

Assuming k_2 to be known, we now calculate the solution $\widehat{\psi}$ to the equation $A \cdot \widehat{\psi} = 0$. Using the first solution of (4.7) in $A \cdot \widehat{\psi} = 0$ implies (see (2) for details):

$$\widehat{\psi}_2 = \frac{c_L k_2}{\sqrt{\omega^2 - c_L^2 k_2^2}}\,\widehat{\psi}_1 \Rightarrow \quad \widehat{\psi}^L := \begin{pmatrix} 1 \\ \frac{c_L k_2}{\sqrt{\omega^2 - c_L^2 k_2^2}} \end{pmatrix} = \begin{pmatrix} 1 \\ \frac{k_2}{k_1} \end{pmatrix}, \tag{4.8}$$

where we denoted by $\widehat{\psi}^L$ the eigenvector of the matrix A for longitudinal waves.Analogous considerations can be carried out when considering the second solution of (4.7), which when used in the second equation of $A \cdot \widehat{\psi} = 0$ implies (see (2) for details):

$$\widehat{\psi}_2 = \frac{k_2^2 c_S^2 - \omega^2}{k_2 c_S \sqrt{\omega^2 - k_2^2 c_S^2}}\,\widehat{\psi}_1 \Rightarrow \quad \widehat{\psi}^{SV} := \begin{pmatrix} 1 \\ \frac{k_2^2 c_S^2 - \omega^2}{k_2 c_S \sqrt{\omega^2 - k_2^2 c_S^2}} \end{pmatrix} = \begin{pmatrix} 1 \\ -\frac{k_1}{k_2} \end{pmatrix}, \tag{4.9}$$

where $\widehat{\psi}^{SV}$ is the eigenvector of the matrix A for in-plane shear waves.

Finally, replacing the expression for u_3 given in (4.4) in (4.3) gives

$$k_1 = \pm\sqrt{\frac{\omega^2}{c_S^2} - k_2^2}. \tag{4.10}$$

Equations (4.7) and (4.10) give rise to the well-known dispersion curves for Cauchy continua for in-plane and out-of-plane waves (see Fig. 2).

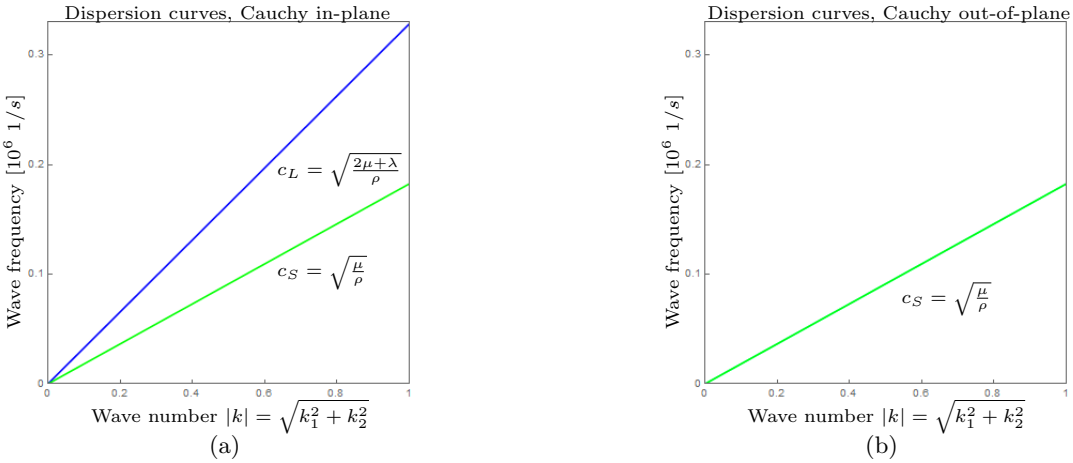

Figure 2: Dispersion diagrams for in-plane (a) and out-of-plane (b) modes in isotropic Cauchy continua. The material parameters used in these Figures are the ones given in Table 4.

Plane-wave ansatz: solution for the displacement field in a Cauchy medium

According to equations (4.4) and considering the 2D eigenvectors (4.8) and (4.9), we can finally write the solution for the displacement field as

$$(u_1, u_2)^{\mathrm{T}} = u^L + u^{SV} = a^L \psi^L e^{i\left(x_1 k_1^L + x_2 k_2^L - \omega t\right)} + a^{SV} \psi^{SV} e^{i\left(x_1 k_1^{SV} + x_2 k_2^{SV} - \omega t\right)} \tag{4.11}$$

when we consider a longitudinal or an SV wave, or

$$u_3 = u^{SH} = a^{SH} \psi^{SH} e^{i\left(x_1 k_1^{SH} + x_2 k_2^{SH} - \omega t\right)}, \tag{4.12}$$

when we consider an SH wave. In these formulas $a^L, a^{SV}, a^{SH} \in \mathbb{C}$ are arbitrary constants and, starting from equations (4.8) and (4.9), we defined the unit vectors

$$\psi^L = \frac{1}{|\widehat{\psi}^L|} \begin{pmatrix} \widehat{\psi}_1^L \\ \widehat{\psi}_2^L \end{pmatrix}, \quad \psi^{SV} = \frac{1}{|\widehat{\psi}^{SV}|} \begin{pmatrix} \widehat{\psi}_1^{SV} \\ \widehat{\psi}_2^{SV} \end{pmatrix}. \tag{4.13}$$

We also explicitly remark that in equations (4.11) and (4.12), k_1^L and k_2^L are related via the first equation of (4.7), k_1^{SV} and k_2^{SV} via the second equation of (4.7) and k_1^{SH} and k_2^{SH} via (4.10).

As we already mentioned, k_2 will be known when imposing boundary conditions, so the only unknowns in the solution (4.11) (resp (4.12)) remain the scalar amplitudes a^L, a^{SV} (resp. a^{SH}) which can be computed by imposing boundary conditions.

4.2. Interface between two Cauchy media

We assume that an incident longitudinal wave[5] propagates on the "minus" side, hits the interface at $x_1 = 0$, is subsequently reflected into an L wave and an SV wave and is transmitted into the second medium on the "plus" side into an L wave and an SV wave as well, according to equations (4.11). If we send an incident SH wave, equation (4.12) tells us that it will reflect and transmit only into SH waves.

[5]The exact same considerations can be carried over when the incident wave is SV transverse.

4.2.1. Incident longitudinal/SV-transverse wave

According to our previous considerations, and given the linearity of the considered problem, the solution of the dynamical problem (2.1) on the "minus" side can be written as[6]

$$(u_1^-, u_2^-)^{\mathrm{T}} = a^{L,i}\psi^{L,i}e^{i\left(\langle x,k^{L,i}\rangle-\omega t\right)}+a^{L,r}\psi^{L,r}e^{i\left(\langle x,k^{L,r}\rangle-\omega t\right)}+a^{SV,r}\psi^{SV,r}e^{i\left(\langle x,k^{SV,r}\rangle-\omega t\right)} =: u^{L,i}+u^{L,r}+u^{SV,r}. \tag{4.14}$$

As for the "plus" side, the solution is

$$(u_1^+, u_2^+)^{\mathrm{T}} = a^{L,t}\psi^{L,t}e^{i\left(\langle x,k^{L,t}\rangle-\omega t\right)} + a^{SV,t}\psi^{SV,t}e^{i\left(\langle x,k^{SV,t}\rangle-\omega t\right)} =: u^{L,t} + u^{SV,t}. \tag{4.15}$$

Now the task is given an incident wave, i.e. knowing $a^{L,i}$ and $k^{L,i}$, to calculate all the respective parameters of the "new" waves. Using (4.15) and (4.14) in the first component of the jump condition (3.1) (which is evaluated at $x_1 = 0$), we get:

$$a^{L,i}\psi_1^{L,i}e^{ix_2k_2^{L,i}} + a^{L,r}\psi_1^{L,r}e^{ix_2k_2^{L,r}} + a^{SV,r}\psi_1^{SV,r}e^{ix_2k_2^{SV,r}} = a^{L,t}\psi_1^{L,t}e^{ix_2k_2^{L,t}} + a^{SV,t}\psi_1^{SV,t}e^{ix_2k_2^{SV,t}}. \tag{4.16}$$

This must hold for all $x_2 \in \mathbb{R}$. The exponentials in this expression form a family of linearly independent functions and, therefore, we can assume that the coefficients $a^{L,i}$, $a^{L,r}$, $a^{SV,r}$, $a^{L,t}$, $a^{SV,t}$ are never all zero simultaneously. This means, than in order for (4.16) to hold, we must require that the exponents of the exponentials are all equal to one another. Canceling out the imaginary unit i and x_2, we deduce the fundamental relation

$$\boxed{k_2^{L,i} = k_2^{L,r} = k_2^{SV,r} = k_2^{L,t} = k_2^{SV,t}}, \tag{4.17}$$

which is the well-known **Snell's law** for in-plane waves (see (1; 3; 14; 46)).

Using (4.17) we see that the exponentials in (4.16) can be canceled out leaving only

$$a^{L,i}\psi_1^{L,i} + a^{L,r}\psi_1^{L,r} + a^{SV,r}\psi_1^{SV,r} = a^{L,t}\psi_1^{L,t} + a^{SV,t}\psi_1^{SV,t}. \tag{4.18}$$

Analogously, equating the second components of the displacements in the jump conditions (3.1), using (4.17) and the fact that this must hold for all $x_2 \in \mathbb{R}$, gives

$$a^{L,i}\psi_2^{L,i} + a^{L,r}\psi_2^{L,r} + a^{SV,r}\psi_2^{SV,r} = a^{L,t}\psi_2^{L,t} + a^{SV,t}\psi_2^{SV,t}. \tag{4.19}$$

As for the jump of traction, we remark that the total traction on both sides is $F^- = t^{L,i} + t^{L,r} + t^{SV,r}$, $F^+ = t^{L,t} + t^{SV,t}$, with the t's being evaluated at $x_1 = 0$. The tractions are vectors of the form

$$t = (t_1, t_2)^T, \qquad \text{with} \qquad t_i = \sigma_{ij}\nu_j, \quad i = 1, 2,\ j = 1, 2, 3, \tag{4.20}$$

where $\nu = (\nu_1, \nu_2, \nu_3)^T = (1, 0, 0)^T$ is the normal vector to the interface, i.e. to the x_2 axis.

The traction jump condition can now be written component-wise as

$$\sigma_{11}^{L,i} + \sigma_{11}^{L,r} + \sigma_{11}^{SV,r} = \sigma_{11}^{L,t} + \sigma_{11}^{SV,t}, \qquad \sigma_{21}^{L,i} + \sigma_{21}^{L,r} + \sigma_{21}^{SV,r} = \sigma_{21}^{L,t} + \sigma_{21}^{SV,t}. \tag{4.21}$$

[6] With a clear extension of the previously introduced notation, we denote by $a^{L,i}, a^{L,r}, a^{L,t}, a^{SV,r}, a^{SV,t}$ and $\psi^{L,i}, \psi^{L,r}, \psi^{L,t}, \psi^{SV,r}, \psi^{SV,t}$ the amplitudes and eigenvectors of longitudinal incident, reflected, transmitted, in-plane transverse incident, reflected and transmitted waves respectively. Analogously, $a^{SV,i}$ and $\psi^{SV,i}$ will denote the amplitude and eigenvector related to in-plane transverse incident waves.

Calculating the stresses according to eq. (2.1), where we use the solutions (4.14) and (4.15) for the displacement and again using (4.17) gives

$$\begin{aligned} &a^{L,i}\left((2\mu+\lambda)\psi_1^{L,i}k_1^{L,i}+\lambda\psi_2^{L,i}k_2^{L,i}\right)+a^{L,r}\left((2\mu+\lambda)\psi_1^{L,r}k_1^{L,r}+\lambda\psi_2^{L,r}k_2^{L,r}\right)\\ &\quad+a^{SV,r}\left((2\mu+\lambda)\psi_1^{SV,r}k_1^{SV,r}+\lambda\psi_2^{SV,r}k_2^{SV,r}\right)\\ &\quad=a^{L,t}\left((2\mu^{+}+\lambda^{+})\psi_1^{L,t}k_1^{L,t}+\lambda^{+}\psi_2^{L,t}k_2^{L,t}\right)+a^{SV,t}\left((2\mu^{+}+\lambda^{+})\psi_1^{SV,t}k_1^{SV,t}+\lambda^{+}\psi_2^{SV,t}k_2^{SV,t}\right), \end{aligned} \tag{4.22}$$

and

$$\begin{aligned} &a^{L,i}\mu\left(\psi_1^{L,i}k_2^{L,i}+\psi_2^{L,i}k_1^{L,i}\right)+a^{L,r}\mu\left(\psi_1^{L,r}k_2^{L,r}+\psi_2^{L,r}k_1^{L,r}\right)+a^{SV,r}\mu\left(\psi_1^{SV,r}k_2^{SV,r}+\psi_2^{SV,r}k_1^{SV,r}\right)\\ &=a^{L,t}\mu^{+}\left(\psi_1^{L,t}k_2^{L,t}+\psi_2^{L,t}k_1^{L,t}\right)+a^{SV,t}\mu^{+}\left(\psi_1^{SV,t}k_2^{SV,t}+\psi_2^{SV,t}k_1^{SV,t}\right). \end{aligned} \tag{4.23}$$

Thus, equations (4.18), (4.19), (4.22), (4.23) form an algebraic system for the unknown amplitudes $a^{L,r}$, $a^{SV,r}$, $a^{L,t}$, $a^{SV,t}$ from which we can fully calculate the solution.

4.2.2. Incident SH-transverse wave

In this case, the solution on the "minus" side of the interface is

$$u_3^{-}=a^{SH,i}\psi^{SH,i}e^{i\left(\langle x,k^{SH,i}\rangle-\omega t\right)}+a^{SH,r}\psi^{SH,r}e^{i\left(\langle x,k^{SH,r}\rangle-\omega t\right)}, \tag{4.24}$$

and on the "plus" side

$$u_3^{+}=a^{SH,t}\psi^{SH,t}e^{i\left(\langle x,k^{SH,t}\rangle-\omega t\right)}. \tag{4.25}$$

Following the same reasoning as in section 4.2.1, the continuity of displacement condition now only involves the u_3 component, which is the only non-zero one, and reads (evaluating again at $x_1=0$)

$$a^{SH,i}e^{i\left(x_2k_2^{SH,i}\right)}+a^{SH,r}e^{i\left(x_2k_2^{SH,r}\right)}=a^{SH,t}e^{i\left(x_2k_2^{SH,t}\right)}, \tag{4.26}$$

which, as before, implies the **Snell's law** for out-of-plane motions

$$\boxed{k_2^{SH,i}=k_2^{SH,r}=k_2^{SH,t}}. \tag{4.27}$$

Using that, we see that the exponentials in (4.26) cancel out leaving only

$$a^{SH,i}+a^{SH,r}=a^{SH,t}. \tag{4.28}$$

As for the jump of traction in the case of SH waves, the total traction on both sides is $F^{-}={t_3}^{SH,i}+{t_3}^{SH,r}$, $F^{+}={t_3}^{SH,t}$, with the t_3's being evaluated at $x_1=0$ and given by $t_{3i}=\sigma_{3j}\nu_j$, where $\nu=(1,0,0)^T$ is the vector normal to the interface. The jump of force can now be written as

$$\sigma_{31}^{SH,i}+\sigma_{31}^{SH,r}=\sigma_{31}^{SH,t} \tag{4.29}$$

The stresses are calculated again by (2.1) and using the solutions (4.25) and (4.24) for the displacement and together with (4.27) gives

$$\mu\left(a^{SH,i}k_1^{SH,i}+a^{SH,r}k_1^{SH,r}\right)=\mu^{+}a^{SH,t}k_1^{SH,t}. \tag{4.30}$$

Equations (4.28) and (4.30) build a system for the unknown amplitudes $a^{SH,r}, a^{SH,t}$, which we can solve and fully determine the solution to the reflection-transmission problem.

4.2.3. Conditions for the onset of Stoneley waves at a Cauchy/Cauchy interface

In this subsection we show how we can find explicit conditions for the onset of Stoneley waves at Cauchy/Cauchy interfaces. Assume that the incident wave is longitudinal. This means that its speed is given by $c_L^- = \sqrt{(2\mu^- + \lambda^-)/\rho^-}$ and that the wave vector k can now be written as $k = (k_1, k_2) = |k|(\sin\theta_i, -\cos\theta_i)$, where $|k| = \omega/c_L^-$ and θ_i is the angle of incidence. As we know, this incident wave gives rise to a longitudinal and a transverse wave both on the "$-$" and on the "$+$" side. Setting the quantity under the square root in the first equation in (4.7) to be negative and using the fact that $k_2 = -|k|\cos\theta_i$, gives a condition for the appearance of Stoneley waves in the case of an incident longitudinal wave:

$$\frac{\omega^2}{(c_L^+)^2} - k_2^+ < 0 \Leftrightarrow \frac{\omega^2}{(c_L^+)^2} - k_2^2 < 0 \Leftrightarrow \frac{\omega^2}{(c_L^+)^2} < |k|^2\cos^2\theta_i$$
$$\Leftrightarrow \frac{\omega^2}{(c_L^+)^2} < \frac{\omega^2}{(c_L^-)^2}\cos^2\theta_i \Leftrightarrow \cos^2\theta_i > \left(\frac{c_L^-}{c_L^+}\right)^2 \Leftrightarrow \cos^2\theta_i > \frac{\rho^+(2\mu^- + \lambda^-)}{\rho^-(2\mu^+ + \lambda^+)}. \tag{4.31}$$

To obtain (4.31) we also used the fact that $k_2^+ = k_2$, as established by **Snell's law** in (4.17).

Similar arguments can be carried out when considering all other possibilities for incident, transmitted and reflected waves, as detailed in Tables 1 and 2.

Incident Wave	Transmitted L	Transmitted SV	Transmitted SH
L	$\cos^2\theta_i > \frac{\rho^+(2\mu^-+\lambda^-)}{\rho^-(2\mu^+ + \lambda^+)}$	$\cos^2\theta_i > \frac{\rho^+(2\mu^-+\lambda^-)}{\rho^-\mu^+}$	–
SV	$\cos^2\theta_i > \frac{\rho^+\mu^-}{\rho^-(2\mu^+ + \lambda^+)}$	$\cos^2\theta_i > \frac{\rho^+\mu^-}{\rho^-\mu^+}$	–
SH	–	–	$\cos^2\theta_i > \frac{\rho^+\mu^-}{\rho^-\mu^+}$

Table 1: Conditions for appearance of transmitted Stoneley waves at a Cauchy/Cauchy interface.

Incident Wave	Reflected L	Reflected SV
L	–	–
SV	$\cos^2\theta_i > \frac{\mu^-}{2\mu^- + \lambda^-}$	–
SH	–	–

Table 2: Conditions for appearance of reflected Stoneley waves at a Cauchy/Cauchy interface.

The conditions in Tables 1 and 2 establish that the square of the cosine of the angle of incidence must be greater than a given quantity for Stoneley waves to appear. This means that it is most likely to observe Stoneley waves when the angle of incidence is smaller than the normal incidence angle, i.e. for incident waves which are inclined with respect to the surface upon which they hit. Moreover, if there exists a strong contrast in stiffness between the two sides and the "$-$" side is by far stiffer than the "$+$" side, then Stoneley waves could be observed for angles closer to normal incidence. On the other hand, if the "$-$" side is only slightly stiffer than the "$+$" side, then Stoneley waves will be observed only for smaller angles (far from normal incidence).

4.2.4. Determination of the reflection and transmission coefficients

We introduce the normal flux H_1, according to (2.5), as:

$$H_1 = -\nu \cdot \sigma \cdot u_{,t}, \tag{4.32}$$

where ν is the normal to the interface and σ is defined in (2.1). Based on (4.32), we introduce the time average of the fluxes for incident, reflected and transmitted waves, respectively, as:

$$J^i = \frac{1}{T}\int_0^T H_1^i(x,t)dt, \quad J^r = \frac{1}{T}\int_0^T H_1^r(x,t)dt, \quad J^t = \frac{1}{T}\int_0^T H_1^t(x,t)dt, \tag{4.33}$$

where $H_1^i = H_1^{L,i}$ (or, $H_1^i = H_1^{SV,i}$ if we consider an incident SV wave), $H_1^r = H_1^{L,r} + H_1^{SV,r}$ and $H_1^t = H_1^{L,t} + H_1^{SV,t}$, T being the period of the wave. Then, the **reflection** and **transmission coefficients** are defined as

$$\mathcal{R} = \frac{J^r}{J^t}, \quad \mathcal{T} = \frac{J^t}{J^i}. \tag{4.34}$$

These coefficients tell us what part of the average normal flux of the incident wave is reflected and what part is transmitted; also, since the system is conservative, we must have $\mathcal{R} + \mathcal{T} = 1$.

These coefficients can be rewritten in a form which is more suitable for numerical computations (see e.g. (2)) by noting that[7]

$$\boxed{\frac{1}{T}\int_0^T H_1 dt = \frac{1}{2}\mathrm{Re}\left(\left[(2\mu+\lambda)|\psi_1|^2 k_1 + \lambda\psi_1^*\psi_2 k_2 + \mu\left(\psi_1\psi_2^* k_2 + |\psi_2|^2 k_1\right)\right]|a|^2\,\omega\right)}, \tag{4.35}$$

and[8]

$$\boxed{\frac{1}{T}\int_0^T H_1 dt = \frac{1}{2}\mathrm{Re}\left(\mu k_1 \left|a^{SH}\right|^2 \omega\right)}, \tag{4.36}$$

for L/SV and SH waves, respectively.

5. Reflective properties of a Cauchy/relaxed micromorphic interface

Closely following what was done for the Cauchy case in section 4.1 for the case of the relaxed micromorphic medium, we see that the 12 kinematic variables of the relaxed micromorphic medium decouple again into two in-plane and out-of-plane systems. Making a plane wave ansatz analogous to (4.4) for the 12 unknown fields and replacing it in equations (2.2), we find

$$A_1 \cdot \widehat{\phi} = 0, \qquad A_2 \cdot \widehat{\chi} = 0, \tag{5.1}$$

[7] In formula (4.35), $*$ denotes complex conjugation, ψ_1 and ψ_2 are the two components of the eigenvectors ψ^L or ψ^{SV} given by (4.13) when considering longitudinal or in-plane shear waves, respectively. Moreover, k_2 is the second component of the wave-vector of the incident wave and k_1 is computed using the first or second equation of (4.7), depending on whether the incident wave is L or SV. Finally, $a = a^L$ or $a = a^{SV}$ (see equation (4.11)) is the amplitude of the considered wave, depending on whether it is L or SV, respectively.

[8] In formula (4.36), k_1 is given by (4.10) (k_2 being the second component of the wave-vector of the incident wave) and a^{SH} is the amplitude of the considered out-of-plane wave (see eq. (4.12)).

where $A_1 \in \mathbb{C}^{7\times 7}$, $A_2 \in \mathbb{C}^{5\times 5}$ are the matrices containing the coefficients of the relaxed micromorphic model (similar to (4.5), see (2) for a detailed presentation) for the in-plane and the out-of-plane systems respectively and $\widehat{\phi} \in \mathbb{C}^7$ and $\widehat{\chi} \in \mathbb{C}^5$ are the corresponding amplitude vectors.

We now look for non-trivial solutions of the equations (5.1). To that end, we impose $\det A_1 = 0$ and $\det A_2 = 0$. Once again, we fix the second component k_2 (resp. $\widetilde{k}_2$) of the wave-vector and solve these equations with respect to k_1 (resp. $\widetilde{k}_1$).[9] The expressions for the solutions of these equations are quite complex and we do not present them explicitly here. As discussed before, we find five and four solutions for the in-plane problem and for the out-of-plane problem, respectively:

$$\pm\, k_1^{(1)}(k_2,\omega),\ \pm k_1^{(2)}(k_2,\omega),\ \pm k_1^{(3)}(k_2,\omega),\ \pm k_1^{(4)}(k_2,\omega),\ \pm k_1^{(5)}(k_2,\omega), \tag{5.2}$$

$$\pm\, \widetilde{k}_1^{(1)}(\widetilde{k}_2,\omega),\ \pm \widetilde{k}_1^{(2)}(\widetilde{k}_2,\omega),\ \pm \widetilde{k}_1^{(3)}(\widetilde{k}_2,\omega),\ \pm \widetilde{k}_1^{(4)}(\widetilde{k}_2,\omega). \tag{5.3}$$

If we plot the functions $\omega = \omega(|k|)$, with $|k| = \sqrt{k_1^2 + k_2^2}$, associated to (5.2) and (5.3), we obtain the in-plane and out-of-plane dispersion curves for the relaxed micromorphic model (see Fig. 3).

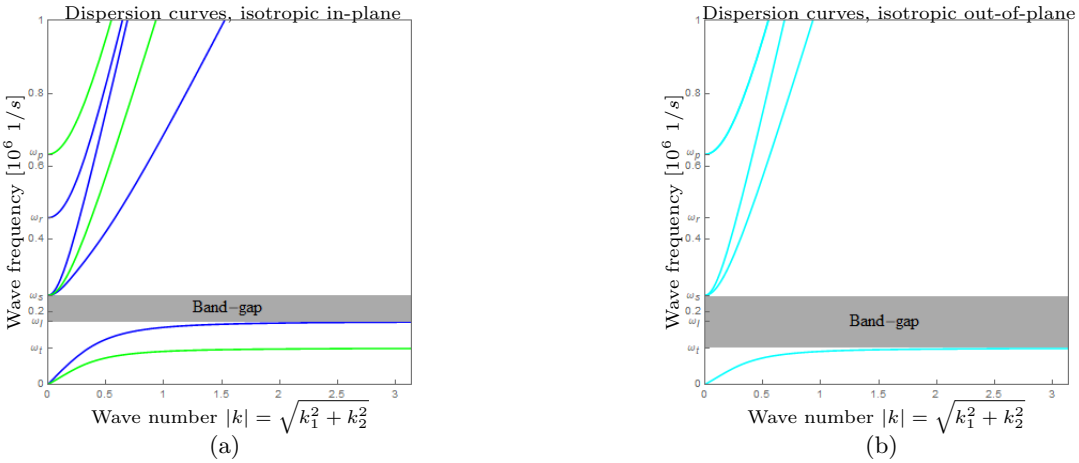

Figure 3: Dispersion diagrams for in-plane (a) and out-of-plane (b) modes in isotropic relaxed micromorphic continua. The material parameters used in these Figures are the ones given in Table 3.

By directly comparing Figures 3 to 2, the extent to which the relaxed micromorphic model generalizes the classical Cauchy framework becomes immediately evident. Seven modes are described for in-plane motion and five (two are superimposed) for out-of-plane. This means that some of the five (resp. four) solutions in (5.2) (resp. (5.3)) have multiple branches when plotted in the $(|k|,\omega)$ plane. The relaxed micromorphic model is able to capture the main macroscopic characteristics of complex mechanical metamaterials, including low- and high-frequency dispersion and band-gaps. It can be automatically verified that, for a wave which propagates in a direction orthogonal to the Cauchy/relaxed micromorphic interface, a sort of uncoupling exists among the in-plane modes in Fig. 3(a). Green modes are activated by an SV incident wave, while blue modes are activated by an

[9] We will show that also in the case of an interface between a Cauchy and a relaxed micromorphic medium, the component k_2 of the wave-vector can be considered to be known when imposing boundary conditions.

L incident wave. This uncoupling is lost for all other directions of propagation, but we can assume, making a small error, it still holds for angles close to normal incidence.

We plug the solutions (5.2) (resp. (5.3)) of the characteristic polynomials into the matrix A_1 (resp. A_2) and calculate for each different k (resp. $\widetilde{k}$) the five (resp. four) nullspaces of the matrix. We find

$$\widehat{\phi}^{(1)}, \widehat{\phi}^{(2)}, \widehat{\phi}^{(3)}, \widehat{\phi}^{(4)}, \widehat{\phi}^{(5)}, \qquad \widehat{\chi}^{(1)}, \widehat{\chi}^{(2)}, \widehat{\chi}^{(3)}, \widehat{\chi}^{(4)}, \tag{5.4}$$

as solutions to the equations $A_1 \cdot \widehat{\phi} = 0$ and $A_2 \cdot \widehat{\chi} = 0$, respectively. We normalize these vectors, thus introducing the normal vectors

$$\phi^{(i)} = \frac{1}{|\widehat{\phi}^{(i)}|}\widehat{\phi}^{(i)}, \qquad \chi^{(j)} = \frac{1}{|\widehat{\chi}^{(j)}|}\widehat{\chi}^{(j)}, \tag{5.5}$$

$i = 1, \dots 5$, $j = 1, \dots 4$. Finally, we can write the solution to equations (2.2) as

$$v^1 = \sum_{i=1}^{5} \alpha_i \phi^{(i)} e^{i\left(\langle x, k^{(i)}\rangle - \omega t\right)}, \quad v^2 = \sum_{j=1}^{4} \beta_i \chi^{(j)} e^{i\left(\langle x, \widetilde{k}^{(j)}\rangle - \omega t\right)}, \tag{5.6}$$

where $\alpha_i, \beta_j \in \mathbb{C}$ for $i = 1, \dots 5$, $j = 1, \dots, 4$ are the unknown amplitudes of the different modes of propagation and $v^1 \in \mathbb{C}^7, v^2 \in \mathbb{C}^5$ collect the 12 kinematical unknowns (see AppendixA and (2) for details).

We explicitly remark that expressions (5.2) and (5.3) for the first component k_1 and $\widetilde{k}_1$ of the wave-vectors, can give rise to different scenarios when varying the value of the frequency ω and the material parameters. As a matter of fact, we briefly remarked before that k_2 can be considered to be known when imposing jump conditions. Indeed, following analogous steps to those performed to obtain equation (4.17) for the interface between two Cauchy media, we can impose the continuity of displacements between a Cauchy and a relaxed micromorphic medium. Considering the first component of the vector equation for the continuity of displacement and using the plane-wave ansatz, one can find, when imposing a longitudinal incident wave

$$\boxed{k_2^{L,i} = k_2^{L,r} = k_2^{SV,r} = k_2^{(1),t} = k_2^{(2),t} = k_2^{(3),t} = k_2^{(4),t} = k_2^{(5),t}.} \tag{5.7}$$

Generalized in-plane Snell's law

On the other hand, when imposing an out-of-plane shear incident wave, the continuity of displacement at the interface gives

$$\boxed{k_2^{SH,i} = k_2^{SH,r} = \widetilde{k}_2^{(1),t} = \widetilde{k}_2^{(2),t} = \widetilde{k}_2^{(3),t} = \widetilde{k}_2^{(4),t}.} \tag{5.8}$$

Generalized out-of-plane Snell's law

Equations (5.7) and (5.8) tell us that, when fixing the incident wave in the Cauchy medium to be longitudinal ($k_2^{L,i}$ known), in-plane shear ($k_2^{SV,i}$ known) or out-of-plane shear ($k_2^{SH,i}$ known), the second components of all the reflected and transmitted wave-vectors are known. They are the **generalized Snell's law** for the case of a Cauchy/relaxed micromorphic interface. As before, this traces two possible scenarios, given that the value of k_2 for the incident wave is always supposed to be real and positive (propagative wave)

1. both k_1 and k_2 (resp. $\widetilde{k}_1, \widetilde{k}_2$) are real (when computing k_1 or $\widetilde{k}_1$ via (5.2) or (5.3) respectively) so that one has propagative waves.

2. k_2 (resp. $\widetilde{k}_2$) is real and k_1 (resp. $\widetilde{k}_1$), when computed via (5.2) (resp. (5.3)) is imaginary, so that one has Stoneley waves propagating only along the interface and decaying away from it.

Depending on the values of the parameters, each of the five in-plane waves, or of the four out-of-plane waves, can be either propagative or Stoneley. Stoneley waves can appear both for low and for high-frequency modes.

5.1. Reflection and transmission coefficients at a Cauchy/relaxed micromorphic interface

According to our definition (2.6), the normal component of the energy flux for a relaxed micromorphic medium is:

$$\widetilde{H}_1 := -\nu \cdot \widetilde{\sigma}^T \cdot u_{,t} - \nu \cdot \left(m^T \cdot P_{,t}\right) : \varepsilon = -u_{i,t}\widetilde{\sigma}_{i1} - m_{ih}P_{ij,t}\varepsilon_{jh1}. \tag{5.9}$$

This expression for the normal flux is the central point of the present paper. Indeed, when compared to (4.32), we see that it generalizes the classical Cauchy flux for two reasons. First, the stress $\widetilde{\sigma}$, which acts on the macroscopic velocity $u_{,t}$, is an "enriched" stress which intrinsically accounts for the effect of the microstructure on the global deformation of the continuum (see (2.3)). Second, we observe a completely new term which consists of the hyper-stress m acting on the micro-strain rate $P_{,t}$. While the generalized stress $\widetilde{\sigma}$ carries the biggest part of the reflection at the interface, the hyper-stress m has a non-negligible effect for strongly non-local metamaterials. An example of such non-local metamaterials is those which exhibit strong contrasts in the stiffnesses of the base materials. The normal flux (5.9) is the interface counterpart of the bulk energy conservation (2.6) and, as such, its continuity at the interface is automatically guaranteed as long as the correct boundary conditions are imposed at the interface. This is indeed true when imposing the jump conditions (3.4) or (3.5). This means that the normal flux $\widetilde{H}_1$ can be used to define the transmission coefficient in such a way that:

(i) it is able to carry information concerning the microstructure-related transmitted energy,

(ii) it is automatically consistent with the associated bulk equations and boundary conditions,

(iii) last, but most importantly, it is directly defined at the macroscopic (homogenized) level.

Consequently, we infer that the normal flux $\widetilde{H}_1$ is able to carry sophisticated information with the need of only a finite number of modes for the exact verification of the balance of energy at the interface. This provides a different approach compared to the classical homogenization methods, in which the number of modes needed to exactly satisfy surface energy conservation in the framework of classical elasticity is infinite (36; 42; 43).

The normal flux $\widetilde{H}_1$ can be rewritten in terms of the in-plane and out-of-plane variables v^1 and v^2, respectively as (see AppendixA for the precise definition of the involved quantities):

$$\boxed{\widetilde{H}_1^1 = v^1_{,t} \cdot \left(H^{11} \cdot v^1_{,1} + H^{12} \cdot v^1_{,2} + H^{13} \cdot v^1\right)},$$

and

$$\boxed{\widetilde{H}_1^2 = v^2_{,t} \cdot \left(H^{21} \cdot v^2_{,1} + H^{22} \cdot v^2_{,2} + H^{23} \cdot v^2\right)}.$$

The reflection and transmission coefficients are defined as:

$$\mathcal{R} = \frac{J^r}{J^i}, \quad \mathcal{T} = \frac{J^t}{J^i}, \tag{5.10}$$

where

$$J^i = \frac{1}{T}\int_0^T H^i(x,t)dt, \quad J^r = \frac{1}{T}\int_0^T H^r(x,t)dt, \quad J^t = \frac{1}{T}\int_0^T H^t(x,t)dt, \tag{5.11}$$

with $H^i = H^{L/SV,i}$, $H^r = H^{L,r} + H^{SV,r}$ and $\widetilde{H}^t = \widetilde{H}^1_1$ for the in-plane case and $H^i = H^{SH,i}$, $H^r = H^{SH,r}$ and $\widetilde{H}^t = \widetilde{H}^2_1$ for the out-of-plane case.

The numerical evaluation of $\mathcal{R}$ and $\mathcal{T}$ is performed by using simplified expressions which are shown in AppendixA. Finally, once again we have that $\mathcal{R} + \mathcal{T} = 1$.

In the case of a Cauchy/relaxed micromorphic interface, the dependency of the fluxes on the frequency ω is maintained, something which is not the case in the Cauchy/Cauchy interface.

6. Results

We start by choosing the values for the parameters of the relaxed micromorphic medium as shown in Table 3. We explicitly remark that other values of such parameters could be chosen, which would be more or less close to real metamaterials parameters (12; 21; 22). Nevertheless, the basic results which we want to show in the present paper are not qualitatively affected by this choice since they only depend on the relative stiffness of the two media which are considered on the two sides and not on the absolute values of such stiffnesses.

ρ [kg/m^3]	η [kg/m]	μ_c [Pa]	μ_e [Pa]	μ_{micro} [Pa]	λ_{micro} [Pa]	λ_e [Pa]	L_c [m]
2000	10^{-2}	2×10^9	2×10^8	10^8	10^8	4×10^8	10^{-2}

Table 3: Numerical values of the constitutive parameters chosen for the relaxed micromorphic medium.

We can now use the following exact homogenization formulas, presented in (4; 12), to compute the equivalent macroscopic coefficients of the Cauchy medium which is approximating the relaxed micromorphic medium at low frequencies:

$$\mu_{\text{macro}} = \frac{\mu_e\,\mu_{\text{micro}}}{\mu_e + \mu_{\text{micro}}}, \qquad 2\mu_{\text{macro}} + 3\lambda_{\text{macro}} = \frac{(2\mu_e + 3\lambda_e)(2\mu_{\text{micro}} + 3\lambda_{\text{micro}})}{2(\mu_e + \mu_{\text{micro}}) + 3(\lambda_e + \lambda_{\text{micro}})}. \tag{6.1}$$

Using formulas (6.1), we compute the stiffnesses λ_{macro} and μ_{macro} of the Cauchy medium which is equivalent to the relaxed micromorphic medium of Table 3 in the low-frequency regime, as in the following Table:

ρ [kg/m^3]	λ_{macro} [Pa]	μ_{macro} [Pa]
2000	8.25397×10^7	6.66667×10^7

Table 4: Macro parameters of the equivalent Cauchy medium corresponding to the relaxed medium of Table 3 at low frequencies.

At this point, we will consider the two cases in which the Cauchy medium on the "−" side is stiffer or softer than the equivalent Cauchy medium on the "+" side, as defined in Table 4.

6.1. Cauchy medium which is "stiffer" than the relaxed micromorphic one

We chose the material parameters of the left Cauchy medium to be those presented in Table 5 and we explicitly remark that these values are greater than those of Table 4, which are relative to the equivalent Cauchy medium corresponding to the considered relaxed micromorphic one.

ρ [kg/m^3]	λ [Pa]	μ [Pa]
2000	4×10^8	2×10^8

Table 5: Lamé parameters and mass density of the Cauchy medium on the left side of the considered Cauchy/relaxed micromorphic interface.

For the chosen values of the constitutive parameters, the critical angles of the incident wave giving rise to low-frequency Stoneley waves can be calculated using Tables 1 and 2. They are found to be $\theta^{L,r}_{\text{crit}} = 33\pi/100$ and $\theta^{L,t}_{\text{crit}} = 17\pi/200$ for an incident SV wave. For this choice of parameters, no critical angles appear for incident L or SH waves.

Figure 4 shows the transmission coefficient for the considered Cauchy/relaxed micromorphic interface, as a function of the angle of incidence and of the frequency, when the microstructure is free to move at the interface (P is left arbitrary at the interface). The coloring of this plot (and of the subsequent ones) is such that the dark blue regions mean zero transmission, while the gradual change towards red is the increase in transmission (red being total transmission). Before commenting on the details of the behavior of the transmission coefficient, we recall that the case of free microstructure boundary condition is the only one which allows us to precisely obtain a Cauchy/equivalent Cauchy interface in the low-frequency regime, something which is not possible when imposing the fixed microstructure boundary condition ($P_{ij} = 0,\ i = 2,3,\ j = 1,2,3$) at the interface. As a matter of fact, it is firmly established that a relaxed micromorphic continuum is equivalent to a Cauchy continuum with stiffnesses λ_{macro} and μ_{macro} when considering the low-frequency regime (see (32)), but this is proven only for the bulk medium. When considering an interface between a Cauchy and a relaxed micromorphic medium, the latter will behave exactly as an equivalent Cauchy medium at low frequencies only if the micro-distortion tensor P is left free at the interface. Indeed, this tensor will arrange its values at the interface in order to let the low-frequency reflective properties of the Cauchy/relaxed micromorphic interface be equivalent to those of a Cauchy/equivalent Cauchy interface. On the other hand, if we impose the fixed microstructure boundary conditions, the tangential components of the tensor P are forced to vanish at the interface, so that the effect of the microstructure is artificially introduced in the response of the material even for those low frequencies for which the bulk material would tend to behave as an equivalent Cauchy medium.

Having drawn such preliminary conclusions, we can now comment Figures 4 and 5 in detail. For the set of numerical values of the parameters given in Table 5 and 4, we established that Stoneley waves can appear in the low-frequency regime only when imposing the incident wave to be SV.

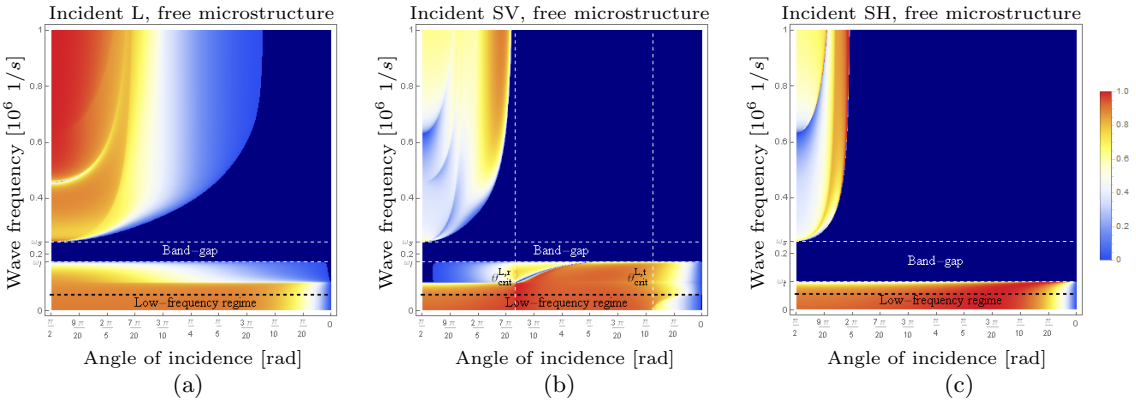

Figure 4: Transmission coefficients as a function of the angle of incidence θ_i and of the wave-frequency ω for L (a), SV (b) and SH (c) incident waves for the case of macro-clamp with free microstructure. The origin coincides with normal incidence ($\theta_i = \pi/2$), while the angle of incidence decreases towards the right until it reaches the value $\theta_i = 0$, which corresponds to the limit case where the incidence is parallel to the interface. The band-gap region is highlighted by two dashed horizontal lines, where, as expected, we observe no transmission. The low-frequency regime is highlighted by the bottom horizontal dashed line, while the critical angles for the onset of Stoneley waves are denoted by vertical dashed lines. The dark blue zone shows that no transmission takes place, while the gradual change from dark blue to red shows the increase of transmission, red being total transmission.

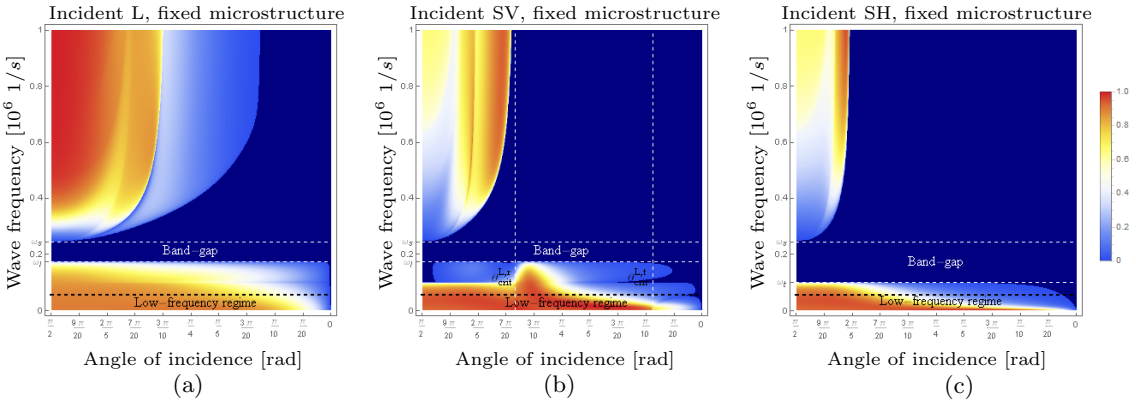

Figure 5: Transmission coefficients as a function of the angle of incidence θ_i and of the wave-frequency ω for L (a), SV (b) and SH (c) incident waves for the case of macro-clamp with fixed microstructure.

In particular, the onset of Stoneley waves in the low-frequency regime can be observed in this case only for longitudinal reflected and transmitted waves when the angles of incidence are beyond $\theta^{L,r}_{\text{crit}}$ and $\theta^{L,t}_{\text{crit}}$, respectively. This fact can be retrieved in Figure 4(b), in which an increase of the transmission coefficient can be observed in the low-frequency regime corresponding to $\theta^{L,r}_{\text{crit}}$ (Stoneley reflected waves are created, producing a decrease of the reflected normal flux and, due to energy conservation, a consequent increase of the transmitted normal flux). On the other hand, we can notice in the same figure a decrease of the transmitted energy in the low-frequency regime beyond the critical angle $\theta^{L,t}_{\text{crit}}$. This is sensible, given that beyond the value of $\theta^{L,t}_{\text{crit}}$, transmitted Stoneley waves are created, which do not contribute to propagative transmitted waves in the relaxed micromorphic continuum. We can also explicitly remark that such a decrease of transmitted energy beyond $\theta^{L,t}_{\text{crit}}$ in the low-frequency regime is much more pronounced than in the corresponding Figures 4(a) and

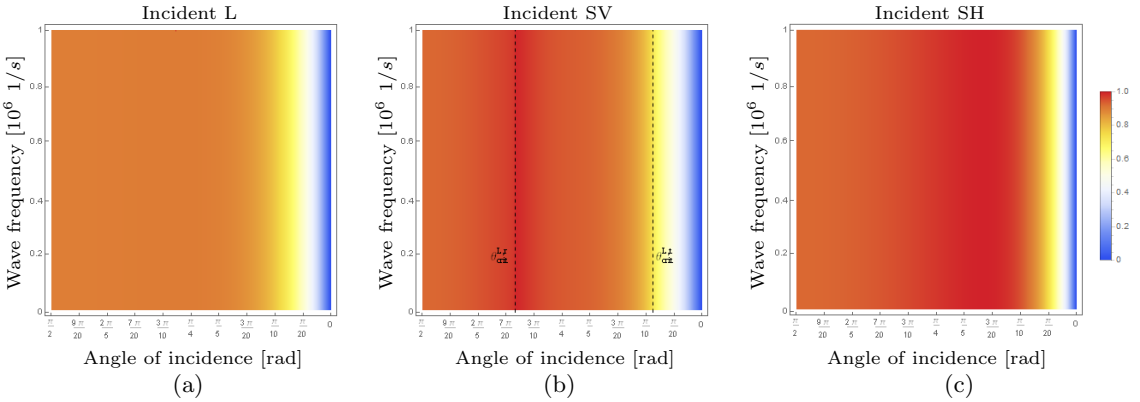

Figure 6: Transmission coefficients as a function of the angle of incidence θ_i and of the wave-frequency ω for L (a), SV (b) and SH (c) incident waves for the case of a Cauchy/Cauchy interface. The parameters of the left Cauchy continuum are given in Table 5, while the ones of the right Cauchy medium are given in Table 4.

4(c). This means that the creation of transmitted Stoneley waves contributes to a decrease of the transmitted energy in the low-frequency regime, but a decreasing trend for the transmission coefficient is observed also for the other cases, when considering angles which are far from normal incidence. This goes along the common feeling, according to which the more inclined the incident wave is with respect to the interface, the less transmission one can expect. The same behavior, even if qualitatively and quantitatively different, can be found in Figure 5(b), in which an increase of transmission can be observed after $\theta^{L,r}_{\text{crit}}$ and a decrease after $\theta^{L,t}_{\text{crit}}$, also for the case of fixed microstructure boundary conditions.

Direct comparison of Figures 4 and 5 allows us to identify the effect that the chosen type of boundary conditions has on the transmission properties of the interface. We already remarked that, at low frequencies, common trends can be identified which are related to critical angles determining the onset of Stoneley waves at the Cauchy/equivalent Cauchy interface. Nevertheless, some differences can also be remarked which are entirely related to the choice of boundary conditions. Surprisingly, the effect of boundary conditions intervenes already for low frequencies, meaning that the fact of imposing the value of P at the interface introduces a tangible effect of the interface microstructured properties on the overall behavior of the considered system. In particular, we can notice that the fact of forcing the tangential part of P to vanish at the interface globally reduces the low-frequency transmission for angles which are much closer to normal incidence, than for the case of free microstructure. This means that the fact of considering a microstructure which is not free to vibrate at the interface, allows for microstructure-related reflections, even if the frequency is relatively low. Such additional reduction of transmission takes place for incident waves which are very inclined with respect to the surface ($\theta_i \leq \pi/4$).

For the sake of completeness and in order to immediately visualize the extent to which the relaxed micromorphic model generalizes the classical setting of linear elasticity, Figure 6 shows the analogous transmission coefficients for the case of a Cauchy/Cauchy interface. These coefficients are obtained for a Cauchy medium on the right, which is the low-frequency limit of the relaxed micromorphic continuum of Fig. 4. It is immediately evident that a reasonable agreement is observed only with the very low frequency regime of Figures 4 and 5. Given that in Cauchy elasticity the transmission coefficient does not depend on the frequency, all other effects at higher frequencies are lost, well before the band-gap region.

Up to now, we only discussed the transmittive properties of the considered Cauchy/relaxed micromorphic interface on the low-frequency regime. Some of the features that we discussed on Stoneley waves can be retrieved by observing Figures 7, 8 and 9 in which the plots of the imaginary part of the first component of the wave vector k_1 are given for each mode of the relaxed micromorphic medium, for L, SV and SH incident waves respectively.

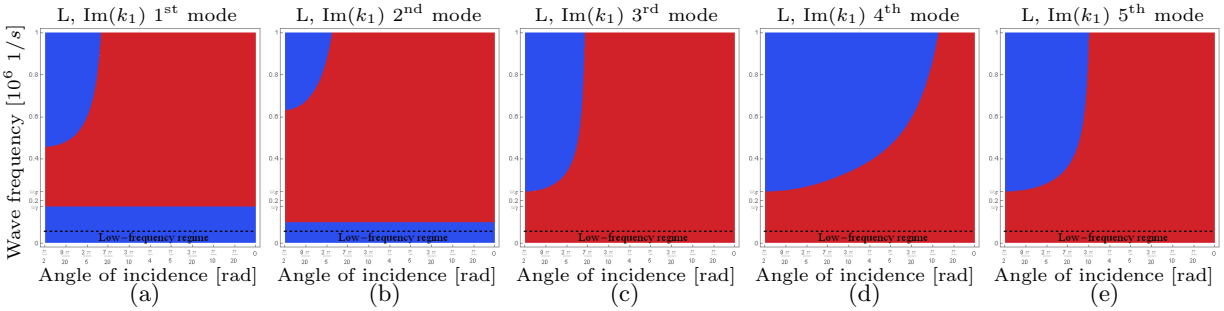

Figure 7: Values of $\mathrm{Im}(k_1)$ as a function of the angle of incidence θ_i and of the wave-frequency ω for the five modes of the relaxed micromorphic medium and for the case of an incident L wave. The origin coincides with normal incidence ($\theta_i = \pi/2$), while the angle of incidence decreases towards the right until it reaches the value $\theta_i = 0$, which corresponds to the limit case where the incidence is parallel to the interface. The first two modes (a) and (b) correspond to the L and SV modes for the equivalent Cauchy continuum at low frequencies. The red color in these plots means that the mode is Stoneley and does not propagate, while blue means that the mode is propagative.

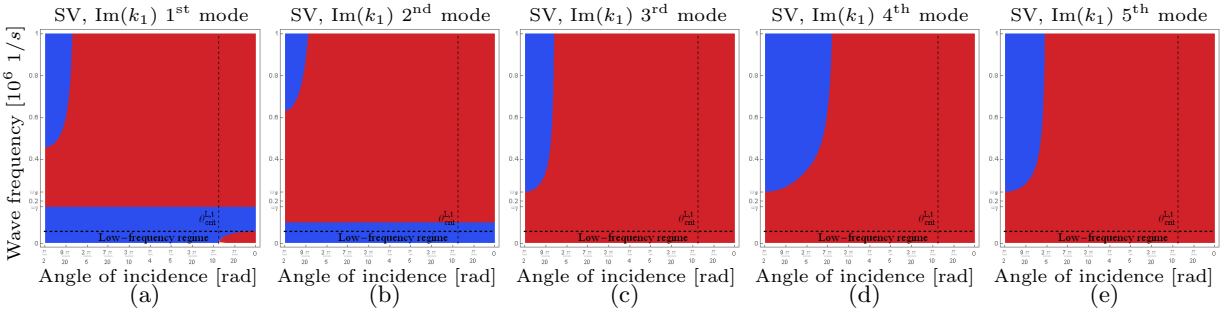

Figure 8: Values of $\mathrm{Im}(k_1)$ as a function of the angle of incidence θ_i and of the wave-frequency ω for the five modes of the relaxed micromorphic medium and for the case of an incident SV wave.

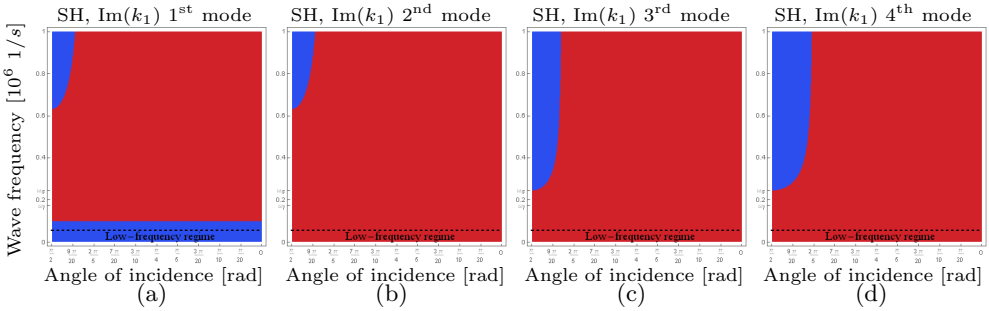

Figure 9: Values of $\mathrm{Im}(k_1)$ as a function of the angle of incidence θ_i and of the wave-frequency ω for the four modes of the relaxed micromorphic medium and for the case of an incident SH wave.

The blue region denotes $\mathrm{Im}(k_1) = 0$ (which implies that k_1 is real), while $\mathrm{Im}(k_1)$ is not vanishing in the red regions. In other words, we can say that for each mode, the red color means that there are Stoneley waves associated to that mode. The first two modes in Figures 7 and 8 correspond to L and SV Cauchy-like modes, while the first mode in Figure 9 is the SH Cauchy-like mode in the low-frequency regime. Since we are considering a relaxed micromorphic medium, three additional modes with respect to the Cauchy case are present both for the in-plane (Figures 7 and 8) and for the out-of-plane problem (Fig. 9). For the Cauchy-like modes we can observe that at low frequencies they are always propagative, except in the case of an incident SV wave, for which Stoneley longitudinal waves appear beyond $\theta_{\mathrm{crit}}^{L,t}$ (also Stoneley reflected waves can be observed in this case, but we do not present the plots of $\mathrm{Im}(k_1)$ for reflected waves to avoid overburdening. We can note by inspecting Figures 7, 8 and (Fig. 9 that the presence of Stoneley waves at high frequencies is much more widespread than at low frequencies for all 5 (resp. 4) modes.

We can observe by direct observation of Figures 7, 8 and 9 that high-frequency critical angles exist for each mode corresponding to which a transition from Stoneley to propagative waves takes place. The value of such critical angles depends on the frequency for the medium-frequency regime and become constant for higher frequencies. The influence of the existence of such high-frequency critical angles can be directly observed on the patterns of the transmission coefficient in Figures 4 and 5, in which high frequency transmission is observed for angles closer to normal incidence and no transmission is reported for smaller angles due to the simultaneous presence of Stoneley waves for all modes. We can call such zones in which transmission is equal to one "extraordinary transmission regions" (see e.g. (29)). Such extraordinary transmission can be used as a basis for the conception of innovative systems such as selective cloaking and non-destructive evaluation.

We can finally remark that the influence of the choice of boundary conditions on the high-frequency behavior of the transmission coefficient is still present, but do not determine drastic changes on the transmission patterns (see Figures 4 and 5).

6.2. Cauchy medium which is "softer" than the relaxed micromorphic one

In this section we present the reflective properties of a Cauchy/relaxed micromorphic interface for which we consider that the Cauchy medium on the left is "softer" than the relaxed micromorphic medium on the right in the same sense as in the previous section. To that end, we choose the material parameters of the left Cauchy medium to be those presented in Table 6 and we explicitly remark that these values are smaller than those of Table 4.

ρ [kg/m^3]	λ [Pa]	μ [Pa]
2000	2×10^7	0.7×10^7

Table 6: Lamé parameters of the "softer" Cauchy medium on the left side of the considered Cauchy/relaxed micromorphic interface.

With these new parameters we can compute again, following Tables 1 and 2, the critical angles for the appearance of Stoneley waves at low frequencies. They are found to be $\theta_{\mathrm{crit}}^{L,t} = 37\pi/100$ and $\theta_{\mathrm{crit}}^{SV,t} = 49\pi/200$ for an incident L wave (no reflected Stoneley mode), $\theta_{\mathrm{crit}}^{L,r} = 7\pi/20$, $\theta_{\mathrm{crit}}^{L,t} = 11\pi/25$ and $\theta_{\mathrm{crit}}^{SV,t} = 39\pi/100$ for an incident SV wave and $\theta_{\mathrm{crit}}^{SH,t} = 39\pi/100$ for an incident SH wave.

Figures 10 and 11 show the transmission coefficient for the softer Cauchy/relaxed micromorphic interface as a function of the angle of incidence and of frequency for both boundary conditions.

We see that when the incident wave travels in a soft medium and hits the interface separating this medium from a stiffer one, many critical angles exist which determine the onset of Stoneley waves for all types of incident wave at low frequencies. Since many more Stoneley waves are created with respect to the previous case of section 6.1, we would expect less transmission in the low-frequency regime than before. This is indeed the case if we inspect Figures 10 and 11: the presence of low-frequency Stoneley waves induces a wides zero-transmission zone in the low-frequency regime. We can also detect a certain role of boundary conditions in widening these zero-transmission zones when considering the fixed microstructure boundary condition (see Figure 11).

Also in this case of a left "softer" Cauchy medium, we plot in Fig. 12 the analogous transmission coefficient when the right side of the interface is occupied by a Cauchy medium. Again, this Cauchy medium on the right is the homogenized limit of the considered micromorphic material. By directly comparing to Fig. 10, we infer that a reasonable agreement can be observed only for very low frequencies. All other higher frequency effects are lost before the band-gap.

Figures 13, 14 and 15 once again show the imaginary part of the first component of the wave-vector k_1 for each mode of the relaxed micromorphic medium on the right. We see that Stoneley waves are observed almost everywhere both at low and high frequencies, with the exception of angles which are very close to normal incidence. Once again, the blue region denotes $\mathrm{Im}(k_1) = 0$ (which implies that k_1 is real), while $\mathrm{Im}(k_1)$ is not vanishing in the red regions, which means that for each mode, the red color denotes that there are Stoneley waves associated to that mode. The first two modes in Figures 13 and 14 correspond to L and SV Cauchy-like modes, while the first mode in Figure 15 is the SH Cauchy-like mode in the low-frequency regime.

Since we are considering a relaxed micromorphic medium, three additional modes with respect to the Cauchy case are present both for the in-plane (Figures 13 and 14) and for the out-of-plane problem. For this choice of parameters which make the left-side medium "softer" than the corresponding Cauchy medium on the right, we see that the Cauchy-like modes for all incident waves become Stoneley after a critical angle (clearly denoted on the plots with a vertical dashed line). Also Stoneley reflected waves can be observed in this case, but we do not present the plots of $\mathrm{Im}(k_1)$ for reflected waves to avoid overburdening.

We see that it is possible to create an almost perfect total screen, which completely reflects incident waves for almost all angles of incidence and wave frequencies. This extraordinary possibility can be obtained by simply tailoring the properties of the left Cauchy medium which has to be chosen to be suitably softer than the right equivalent Cauchy medium. Regions of extraordinary transmission for very wade ranges of incident angles and wave frequencies can be engineered, opening the door to exciting applications.

Before concluding the Results section, we point out a last interesting property of the transmission coefficient obtained by the relaxed micromorphic model. In both cases (see Figures 4, 5, 10, 11) the band-gap for SV incident waves is more extended than the band-gap for L incident waves for angles close to normal incidence. This phenomenon is due to the uncoupling of L and SV "activated" acoustic modes close to normal incidence outlined in Fig. 3. Close to normal incidence, only the green modes are activated by an incident SV wave, so that the band-gap is widened. This "uncoupling" effect can often be observed in real metamaterials. An analogous "mode uncoupling" at higher frequencies is responsible for the wider zero-transmission high-frequency region for SV incident waves compared to L incident waves.

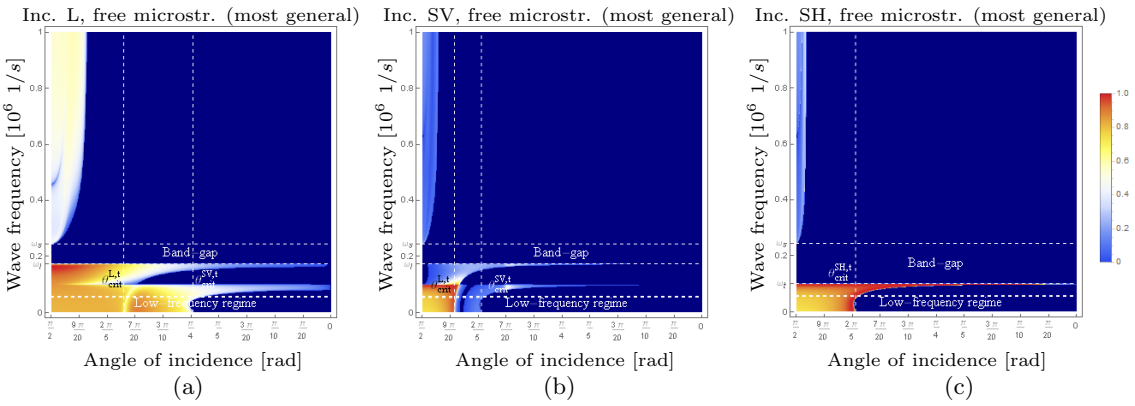

Figure 10: Transmission coefficients as a function of the angle of incidence θ_i and of the wave-frequency ω for L (a), SV (b) and SH (c) incident waves for the case of macro-clamp with free microstructure and for a "softer" Cauchy medium on the left.

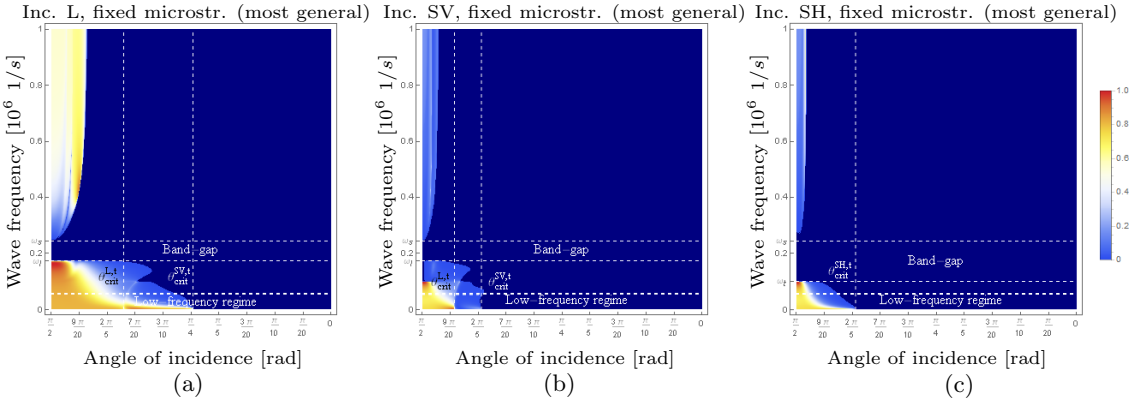

Figure 11: Transmission coefficients as a function of the angle of incidence θ_i and of the wave-frequency ω for L (a), SV (b) and SH (c) incident waves for the case of macro-clamp with fixed microstructure and for a "softer" Cauchy medium on the left.

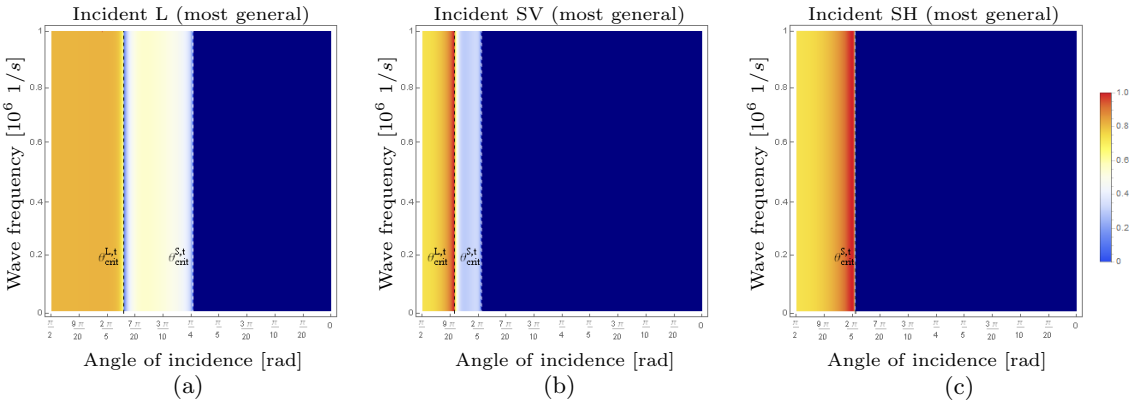

Figure 12: Transmission coefficients as a function of the angle of incidence θ_i and of the wave-frequency ω for L (a), SV (b) and SH (c) incident waves for the case of a Cauchy/Cauchy interface. The parameters of the left Cauchy continuum are given in Table 6, while the ones of the right Cauchy medium are given in Table 4.

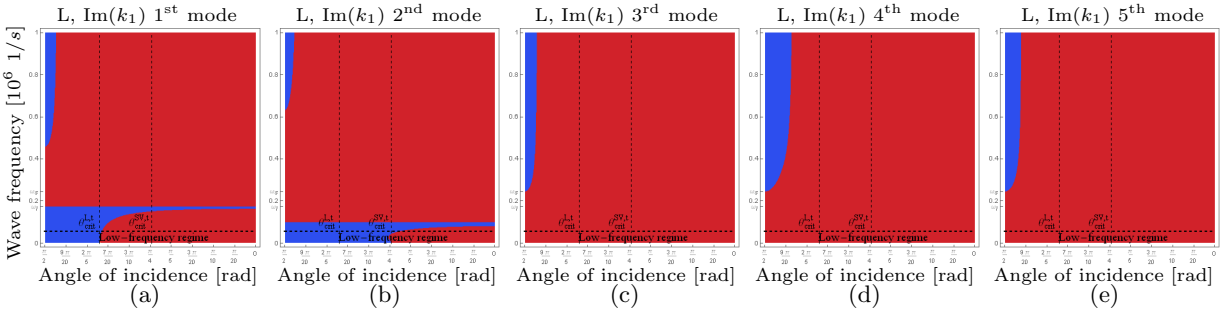

Figure 13: Values of $\mathrm{Im}(k_1)$ as a function of the angle of incidence θ_i and of the wave-frequency ω for the five modes of the relaxed micromorphic medium for the case of an incident L wave and a "softer" Cauchy medium on the left.

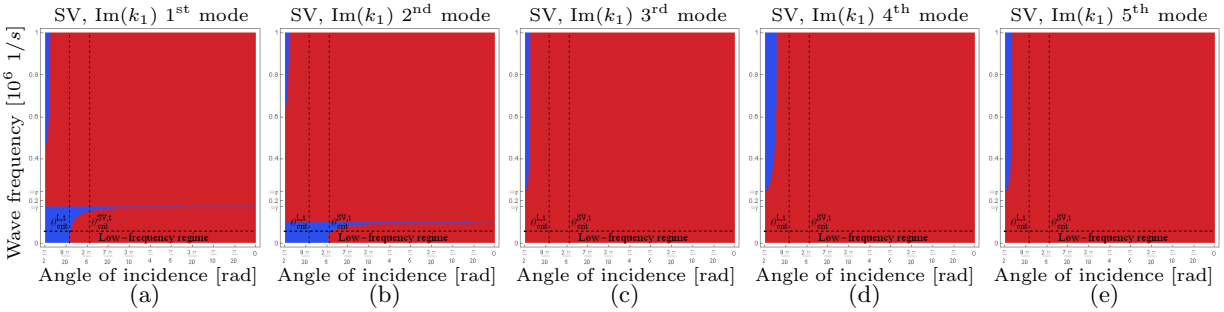

Figure 14: Values of $\mathrm{Im}(k_1)$ as a function of the angle of incidence θ_i and of the wave-frequency ω for the five modes of the relaxed micromorphic medium for the case of an incident SV wave and a "softer" Cauchy medium on the left.

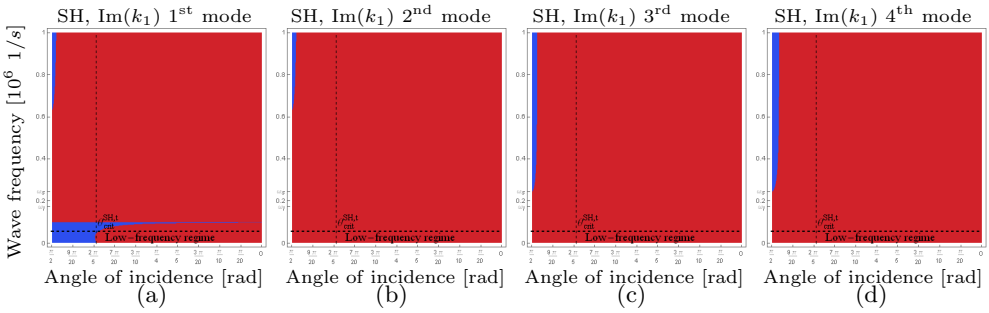

Figure 15: Values of $\mathrm{Im}(k_1)$ as a function of the angle of incidence θ_i and of the wave-frequency ω for the four modes of the relaxed micromorphic medium for the case of an incident SH wave and a "softer" Cauchy medium on the left.

7. Conclusions

In this paper we present the detailed study of the reflective and refractive properties of a two-dimensional interface separating a classical Cauchy medium from a relaxed micromorphic medium. Both media are assumed to be semi-infinite.

We show in great detail that critical angles of incidence exist, beyond which classical Stoneley waves appear at low frequencies. It is shown that these critical angles directly depend on the relative mechanical properties of the two media. Moreover, we unveil the existence of critical angles which

give rise to Stoneley waves at higher frequencies. These Stoneley waves are clearly related to the presence of an underlying microstructure in the metamaterial.

We show that, due to the onset of low and high-frequency Stoneley waves, wide frequency bounds where total reflection and/or total transmission occur can be engineered. This total reflection/transmission phenomenon is appealing for applications, in which total screens for elastic waves, such as cloaks or wave-filters, are desirable. It is clear that the ability of widening the frequency and incident angle intervals for which total reflection/transmission occur, would be of paramount importance for conceiving new devices which are more and more performant for wavefront manipulation.

We also clearly show that the simple fact of suitably tailoring the relative stiffnesses of the two media allows for the possibility of conceiving almost perfect total screens which do not transmit elastic waves for any kind of incident wave (longitudinal, in-plane and out-of-plane shear) and for almost all (low and high) frequencies and angles of incidence. Acting on such relative stiffnesses allows to achieve also the opposite situation, where total transmission occurs for large frequency bounds before a microstructure-related critical angle. This could be exploited for the conception of selective cloaks which make objects transparent to waves dependently on the angle of incidence.

Future work will be devoted to the application of the framework presented here in "real-life" applications, continuing the study of the scattering properties of the interface separating a homogeneous medium from a specific metamaterial with known microstructure. To fully succeed in this plan, we will need to generalize the present isotropic study to the anisotropic setting.

Acknowledgements

Angela Madeo and Domenico Tallarico acknowledge funding from the French Research Agency ANR, "METASMART" (ANR-17CE08-0006). Angela Madeo acknowledges support from IDEX-LYON in the framework of the "Programme Investissement d'Avenir" ANR-16-IDEX-0005. All the authors acknowledge funding from the "Région Auvergne-Rhône-Alpes" for the "SCUSI" project for international mobility France/Germany.

[1] J. D. Achenbach. *Wave Propagation in Elastic Solids*. North-Holland Publishing Company, Amsterdam, The Netherlands, 1973.

[2] A. Aivaliotis, A. Daouadji, G. Barbagallo, D. Tallarico, P. Neff, and A. Madeo. Low-and high-frequency Stoneley waves, reflection and transmission at a Cauchy/relaxed micromorphic interface. *arXiv preprint*, 2018.

[3] B. A. Auld. *Acoustic Fields and Waves in Solids, Vol. II*. Wiley-Interscience Publication, 1973.

[4] G. Barbagallo, A. Madeo, M. V. d'Agostino, R. Abreu, I.-D. Ghiba, and P. Neff. Transparent anisotropy for the relaxed micromorphic model: macroscopic consistency conditions and long wave length asymptotics. *International Journal of Solids and Structures*, 120:7–30, 2017.

[5] C. Bellis and B. Lombard. Simulating transient wave phenomena in acoustic metamaterials using auxiliary fields. *Wave Motion*, 86:175–194, 2019.

[6] T. Bückmann, M. Kadic, R. Schittny, and M. Wegener. Mechanical cloak design by direct lattice transformation. *Proceedings of the National Academy of Sciences*, 112(6):4930–4934, 2015.

[7] G. Chaplain, M. Makwana, and R. Craster. Rayleigh–bloch, topological edge and interface waves for structured elastic plates. *Wave Motion*, 86:162–174, 2019.

[8] H. Chen and C. T. Chan. Acoustic cloaking in three dimensions using acoustic metamaterials . *Applied Physics Letters*, 91, 2007.

[9] R. V. Craster and S. Guenneau. *Acoustic metamaterials: Negative refraction, imaging, lensing and cloaking*, volume 166. Springer Science & Business Media, 2012.

[10] R. V. Craster, J. Kaplunov, and A. V. Pichugin. High-frequency homogenization for periodic media. *Proceedings of the Royal Society A: Mathematical, Physical and Engineering Sciences*, 466(2120):2341–2362, 2010.

[11] S. A. Cummer, J. Christensen, and A. Alú. Controlling sound with acoustic metamaterials. *Nature Reviews Materials*, 113(3), 2014.

[12] M. V. d'Agostino, G. Barbagallo, I.-D. Ghiba, B. Eidel, P. Neff, and A. Madeo. Effective description of anisotropic wave dispersion in mechanical band-gap metamaterials via the relaxed micromorphic model. *submitted, arXiv preprint*, 1709.07054, 2018.

[13] I.-D. Ghiba, P. Neff, A. Madeo, L. Placidi, and G. Rosi. The relaxed linear micromorphic continuum: Existence, uniqueness and continuous dependence in dynamics. *Mathematics and Mechanics of Solids*, 20(10):1171–1197, 2015.

[14] K. F. Graff. *Wave Motion in Elastic Solids*. Dover Publications, Inc., New York, 1975.

[15] S. Guenneau, A. Movchan, G. Pétursson, and S. A. Ramakrishna. Acoustic metamaterials for sound focusing and confinement. *New Journal of Physics*, 9(399), 2007.

[16] N. Kaina, A. Causier, Y. Bourlier, M. Fink, T. Berthelot, and G. Lerosey. Slow waves in locally resonant metamaterials line defect waveguides. *Scientific Reports*, 7(1), 2014.

[17] Y. Li and B. M. Assouar. Acoustic metasurface-based perfect absorber with deep subwavelength thickness . *Applied Physics Letters*, 108(6), 2016.

[18] B. Lieang, J.-c. Chang, and C.-W. Qiu. Wavefront manipulation by acoustic metasurfaces: from physics and applications. *Nanophotonics*, 7(6):1191–1205, 2018.

[19] J.-L. Lions and G. Papanicolaou. *Asymptotic Analysis for Periodic Structures*. AMS Chelsea Publishing, 1978.

[20] Z. Liu, X. Zhang, Y. Mao, Y. Zhu, Z. Yang, C. T. Chan, and P. Sheng. Locally resonant sonic materials. *Science*, 289(5485):1734–1736, 2000.

[21] A. Madeo, G. Barbagallo, M. Collet, M. V. d'Agostino, M. Miniaci, and P. Neff. Relaxed micromorphic modeling of the interface between a homogeneous solid and a band-gap metamaterial: New perspectives towards metastructural design. *Mathematics and Mechanics of Solids*, pages 1–22, 2017.

[22] A. Madeo, G. Barbagallo, M. V. d'Agostino, L. Placidi, and P. Neff. First evidence of non-locality in real band-gap metamaterials: determining parameters in the relaxed micromorphic model. *Proceedings of the Royal Society A: Mathematical, Physical and Engineering Sciences*, 472(2190):20160169, 2016.

[23] A. Madeo, M. Collet, M. Miniaci, K. Billon, M. Ouisse, and P. Neff. Modeling phononic crystals via the weighted relaxed micromorphic model with free and gradient micro-inertia. *Journal of Elasticity*, 130(1):59–83, 2017.

[24] A. Madeo, P. Neff, E. C. Aifantis, G. Barbagallo, and M. V. d'Agostino. On the role of micro-inertia in enriched continuum mechanics. *Proceedings of the Royal Society A: Mathematical, Physical and Engineering Science*, 473(2198):20160722, 2017.

[25] A. Madeo, P. Neff, M. V. d'Agostino, and G. Barbagallo. Complete band gaps including non-local effects occur only in the relaxed micromorphic model. *Comptes Rendus Mécanique*, 344(11-12):784–796, 2016.

[26] A. Madeo, P. Neff, I.-D. Ghiba, L. Placidi, and G. Rosi. Band gaps in the relaxed linear micromorphic continuum. *Zeitschrift für Angewandte Mathematik und Mechanik*, 95(9):880–887, 2014.

[27] A. Madeo, P. Neff, I.-D. Ghiba, L. Placidi, and G. Rosi. Wave propagation in relaxed micromorphic continua: modeling metamaterials with frequency band-gaps. *Continuum Mechanics and Thermodynamics*, 27(4-5):551–570, 2015.

[28] A. Madeo, P. Neff, I.-D. Ghiba, and G. Rosi. Reflection and transmission of elastic waves in non-local band-gap metamaterials: a comprehensive study via the relaxed micromorphic model. *Journal of the Mechanics and Physics of Solids*, 95:441–479, 2016.

[29] D. Misseroni, D. J. Colquitt, A. B. Movchan, N. V. Movchan, and I. S. Jones. Cymatics for the cloaking of flexural vibrations in a structured plate. *Scientific Reports*, 6(23929), 2016.

[30] P. Neff, I.-D. Ghiba, M. Lazar, and A. Madeo. The relaxed linear micromorphic continuum: well-posedness of the static problem and relations to the gauge theory of dislocations. *The Quarterly Journal of Mechanics and Applied Mathematics*, 68(1):53–84, 2015.

[31] P. Neff, I.-D. Ghiba, A. Madeo, L. Placidi, and G. Rosi. A unifying perspective: the relaxed linear micromorphic continuum. *Continuum Mechanics and Thermodynamics*, 26(5):639–681, 2014.

[32] P. Neff, A. Madeo, G. Barbagallo, M. V. d'Agostino, R. Abreu, and I.-D. Ghiba. Real wave propagation in the isotropic-relaxed micromorphic model. *Proceedings of the Royal Society A: Mathematical, Physical and Engineering Sciences*, 473(2197):20160790, 2017.

[33] S. Owczarek, I.-D. Ghiba, M.-V. d'Agostino, and P. Neff. Nonstandard micro-inertia terms in the relaxed micromorphic model: well-posedness for dynamics. *to appear in Mathematics and Mechanics of Solids*, 2018.

[34] L. J. W. S. Rayleigh. On waves propagated along the plane surface of an elastic solid. *Proceedings of the London Mathematical Society*, 17:4–11, 1885.

[35] A. Sridhar, V. G. Kouznetsova, and M. G. Geers. A general multiscale framework for the emergent effective elastodynamics of metamaterials. *Journal of the Mechanics and Physics of Solids*, 111:414–433, 2018.

[36] A. Srivastava and J. R. Willis. Evanescent wave boundary layers in metamaterials and sidestepping them through a variational approach. *Proc. R. Soc. A*, 473(2200):20160765, 2017.

[37] R. Stoneley. Elastic waves at the surface of separation of two solids. *Proceedings of the Royal Society A: Mathematical, Physical and Engineering Sciences*, 106(738):416–428, 1924.

[38] D. Tallarico, N. V. Movchan, A. B. Movchan, and D. J. Colquitt. Tilted resonators in a triangular elastic lattice: Chirality, Bloch waves and negative refraction. *Journal of the Mechanics and Physics of Solids*, 103:236–256, 2017.

[39] D. Tallarico, A. Trevisan, N. V. Movchan, and A. B. Movchan. Edge waves and localization in lattices containing tilted resonators. *Frontiers in Materials*, 4(June):1–13, 2017.

[40] J. Valentine, J. Li, T. Zentgraf, G. Bartal, and X. Zhang. An optical cloak made of dielectrics. *Nature Materials*, 8(7):568–571, 2009.

[41] P. Wang, F. Casadei, S. Shan, J. C. Weaver, and K. Bertoldi. Harnessing buckling to design tunable locally resonant acoustic metamaterials. *Physical Review Letters*, 113, 2014.

[42] J. R. Willis. Dynamics of composites. In *Continuum micromechanics*, pages 265–290. Springer, 1997.

[43] J. R. Willis. Exact effective relations for dynamics of a laminated body. *Mechanics of Materials*, 41(4):385–393, 2009.

[44] Y. Xiao, J. Wen, and X. Wen. Longitudinal wave band gaps in metamaterial-based elastic rods containing multi-degree-of-freedom resonators. *New Journal of Physics*, 14, 2011.

[45] Y. Xie, W. Wang, H. Chen, A. Konneker, B.-I. Popa, and S. A. Cummer. Wavefront modulation and subwavelength diffractive acoustics with an acoustic metasurface. *Nature Communications*, 5(1):1191–1205, 2014.

[46] R. Zhu, X. N. Liu, and G. L. Huang. Study of anomalous wave propagation and reflection in semi-infinite elastic metamaterials. *Wave Motion*, 55:73–83, 2015.

AppendixA. Kinematical variables and energy flux for the relaxed micromorphic model

We proceed to make the following change of variables which are motivated by the Cartan-Lie decomposition of the tensor P:

$$P^S = \frac{1}{3}(P_{11}+P_{22}+P_{33}), \quad P_1^D = P_{11}-P^S, \quad P_2^D = P_{22}-P^S, \quad P_{(1\gamma)} = \frac{1}{2}(P_{1\gamma}+P_{\gamma 1}),$$
$$P_{[1\gamma]} = \frac{1}{2}(P_{1\gamma}-P_{\gamma 1}), \quad P_{(23)} = \frac{1}{2}(P_{23}+P_{32}), \quad P_{[23]} = \frac{1}{2}(P_{23}-P_{32}), \tag{A.1}$$

with $\gamma = 2, 3$. We can then collect the variables which are coupled as

$$v^1 = \left(u_1, u_2, P_1^D, P_2^D, P^S, P_{(12)}, P_{[12]}\right)^T, \qquad v^2 = \left(u_3, P_{(13)}, P_{[13]}, P_{(23)}, P_{[23]}\right)^T. \tag{A.2}$$

The expression (2.6) for the energy flux in the relaxed micromorphic model can be rewritten in terms of the new variables (A.2). The part of the flux involving the in-plane quantity reads:

$$\widetilde{H}_1^1 = v_{,t}^1 \cdot (H^{11} \cdot v_{,1}^1 + H^{12} \cdot v_{,2}^1 + H^{13} \cdot v^1),$$

where

$$H^{11} = \begin{pmatrix} -2\mu_e-\lambda_e & 0 & 0 & 0 & 0 & 0 & 0 \\ 0 & -\mu_e-\mu_c & 0 & 0 & 0 & 0 & 0 \\ 0 & 0 & -L_c^2\mu_e & -L_c^2\mu_e & L_c^2\mu_e & 0 & 0 \\ 0 & 0 & -L_c^2\mu_e & -2L_c^2\mu_e & 0 & 0 & 0 \\ 0 & 0 & L_c^2\mu_e & 0 & -2L_c^2\mu_e & 0 & 0 \\ 0 & 0 & 0 & 0 & 0 & -L_c^2\mu_e & -L_c^2\mu_e \\ 0 & 0 & 0 & 0 & 0 & -L_c^2\mu_e & -L_c^2\mu_e \end{pmatrix}, \tag{A.3}$$

$$H^{12} = \begin{pmatrix} 0 & -\lambda_e & 0 & 0 & 0 & 0 & 0 \\ \mu_c-\mu_e & 0 & 0 & 0 & 0 & 0 & 0 \\ 0 & 0 & 0 & 0 & 0 & 0 & 0 \\ 0 & 0 & 0 & 0 & 0 & L_c^2\mu_e & -L_c^2\mu_e \\ 0 & 0 & 0 & 0 & 0 & L_c^2\mu_e & -L_c^2\mu_e \\ 0 & 0 & L_c^2\mu_e & 0 & L_c^2\mu_e & 0 & 0 \\ 0 & 0 & L_c^2\mu_e & 0 & L_c^2\mu_e & 0 & 0 \end{pmatrix}, \quad H^{13} = \begin{pmatrix} 0 & 0 & 2\mu_e & 0 & 2\mu_e+3\lambda_e & 0 & 0 \\ 0 & 0 & 0 & 0 & 0 & 2\mu_e & -2\mu_c \\ 0 & 0 & 0 & 0 & 0 & 0 & 0 \\ 0 & 0 & 0 & 0 & 0 & 0 & 0 \\ 0 & 0 & 0 & 0 & 0 & 0 & 0 \\ 0 & 0 & 0 & 0 & 0 & 0 & 0 \\ 0 & 0 & 0 & 0 & 0 & 0 & 0 \end{pmatrix}. \tag{A.4}$$

The expression for the energy flux in the relaxed micromorphic model involving out-of-plane-quantities is given by:

$$\widetilde{H}_1^2 = v_{,t}^2 \cdot (H^{21} \cdot v_{,1}^2 + H^{22} \cdot v_{,2}^2 + H^{23} \cdot v^2),$$

where

$$H^{21} = \begin{pmatrix} -\mu_c-\mu_e & 0 & 0 & 0 & 0 \\ 0 & 0 & 0 & 0 & 0 \\ 0 & 0 & 0 & 0 & 0 \\ 0 & 0 & 0 & 0 & 0 \\ 0 & 0 & 0 & -L_c^2\mu_e & L_c^2\mu_e \\ 0 & 0 & 0 & L_c^2\mu_e & -L_c^2\mu_e \end{pmatrix}, \quad H^{22} = \begin{pmatrix} 0 & 0 & 0 & 0 & 0 \\ 0 & 0 & 0 & 0 & 0 \\ 0 & 0 & 0 & 0 & 0 \\ 0 & 0 & 0 & 0 & 0 \\ 0 & L_c^2\mu_e & -L_c^2\mu_e & 0 & 0 \\ 0 & -L_c^2\mu_e & L_c^2\mu_e & 0 & 0 \end{pmatrix}, \tag{A.5}$$

$$H^{23} = \begin{pmatrix} 0 & 2\mu_e & -2\mu_c & 0 & 0 \\ 0 & 0 & 0 & 0 & 0 \\ 0 & 0 & 0 & 0 & 0 \\ 0 & 0 & 0 & 0 & 0 \\ 0 & 0 & 0 & 0 & 0 \\ 0 & 0 & 0 & 0 & 0 \end{pmatrix}. \tag{A.6}$$